Breathing rate and heart rate as confounding factors in measuring T wave alternans and morphological variability in ECG

Ismail Sadiq[1], Erick A Perez-Alday[2], Amit J Shah[3] and Gari D Clifford[2,4]

[1] Department of Electrical & Computer Engineering, Georgia Institute of Technology, Atlanta, GA
[2] Department of Biomedical Informatics, Emory University, Atlanta, GA
[3] Department of Epidemiology, Rollins School of Public Health, Emory University, Atlanta, GA
[4] Department of Biomedical Engineering, Georgia Institute of Technology and Emory University, Atlanta, GA

Keywords – Baseline wander, dynamic time-warping, electrode movement, electrocardiogram, morphological variability, muscle artifacts, repolarization, T wave alternans.

Abstract

Objective: High morphological variability magnitude (MVM) and microvolt T-wave alternans (TWA) within an electrocardiogram (ECG) signifies increased electrical instability and risk of sudden cardiac death. However, the influence of breathing rate (BR), heart rate (HR), and signal-to-noise ratio (SNR) is unknown and may inflate measured values. *Approach*: We synthesize ECGs with morphologies derived from the Physikalisch-Technische Bundesanstalt Database. We calculate MVM and TWA at varying BRs, HRs and SNRs. We compare the MVM and TWA of signal with vs. without breathing at varying HRs and SNRs.We then quantify the percentage of MVM and TWA estimates affected by BR and HR in a healthy population and assess the effect of removing these affected estimates on a method for classifying individuals with and without post-traumatic stress disorder (PTSD). *Main results*: For signals with high SNR (>15 dB), MVM is significantly increased when BRs are $>$ 9 respirations/minute (rpm) and HRs are $<$ 100 beats/minute (bpm). Increased TWAs are detected for HR/BR pairs of 60/15, 60/30 and 120/30 bpm/rpm. For 18 healthy participants, 8.33% of TWA windows and 66.76% of MVM windows are affected by BR and HR. On average, the number of windows with TWA elevations $>$ 47 μV decreases by 23% after excluding regions with significant BR and HR effect. Adding HR and BR to a morphological variability feature increases the classification performance by 6% for individuals with and without PTSD. *Significance*: Physiological BR and HR significantly increase MVM and TWA, indicating that BR and HR should be considered separately as confounders. The code for this work has been released as part of an open-source toolbox.

1 Introduction

Ventricular arrhythmias are one of the leading causes of mortality due to cardiac disease [1]. An important mitigation strategy is an early detection so that timely preventive measures can be taken. A diverse amount of clinical information is also generally incorporated to aid in risk stratification after acute coronary syndrome (ACS). Risk scores like the Global Registry of Acute Coronary Events (GRACE) and Thrombolysis in Myocardial Infarction (TIMI) incorporate cardiac risk factors and biomarker data. However, they only capture a subset of high-risk patients [2], [3]. There is a need to identify the significant number of patients who suffer from similar fatal arrhythmias leading to ACS. Computational biomarkers may present a solution [4].

Morphology changes like T wave alternans (TWA) and ST-segment elevation have been studied extensively to identify possible correlations with arrhythmia onset [5], [6]. Current methods for TWAs detection involve identifying changes in amplitude of adjacent T waves (in an 'ABABAB ... ' pattern). For example, methods like the Modified Moving Average (MMA) [7], look to find TWA, which has a period of 2 beats and characterize T wave variability strictly in terms of amplitude. [8] detect T wave variability with a more complex pattern. Other reported techniques have investigated the surface electrocardiogram (ECG) to measure ventricular repolarization through variations in the T-wave shape [9] and width [10].

Additionally, there has been some attention to QRS morphological variability (MV) in terms of the depolarization of the ECG [4], [11]–[19], and timing variability of the depolarization plus repolarization i.e., the variability of the QT interval [20]and changes in Tpe, (the distance from QRS peak to the end of the T-wave) [21]. However, these studies on MV of the QRS complex are limited compared to MV for T waves. The study detailed in this article attempts to develop a generalized approach to MV for the QRS complex, termed morphological variability magnitude (MVM). Unlike TWA detection, the QRS variability is measured to capture variability in non-binary sequences with a period greater than 2. An established TWA detection technique is also studied [22].

QRS morphological variability and TWA are predictors of heart failure [4], [7]. However, it is unclear whether the elevated changes in the MV of ECG are due to abnormalities in the heart's conduction system or are caused by the irregular breathing rates of the subjects. Cheyne-Stokes breathing is an abnormal breathing pattern that commonly occurs in patients with congestive heart failure (CHF) [23]. Increased MV has also been shown to be a predictor of heart failure [4]. It is well known that the amplitudes of each component of the ECG change with breathing effort and nonstationary noise [24], [25]. In earlier works, we demonstrated that heart rate (HR) dependence at varying breathing rates (BR) significantly affected TWA measurements, particularly in sleep, where breathing patterns are observed [26]. These HRs may have falsely triggered elevated TWA estimates any published noise thresholding approaches may not have rejected. It is unclear if these effects contribute to MV. In particular, periodic breathing that is approximately a multiple of heart rate may cause elevated MVM, rather than abnormalities in the heart's conduction system. Previous studies have not considered this breathing-heart rate interaction effect as a confounding factor. The coupled effect of HR and BR may have led to an over-estimate of MVM and TWA, hence affecting the predictive value and clinical utility of these metrics.

We hypothesize that poor signal quality and high BRs, at various heart rates, will artificially inflate the quantification of MV in the signal. To evaluate our hypothesis, state of the art TWA and MVM estimation algorithms are tested on simulated ECG data for varying breathing rates and heart rates, to test physiological conditions that may lead to false-positive detection. They are also tested under varying signal-to-noise ratios (SNR) to test noise contamination conditions that may cause false-positive detection. The algorithms are used to evaluate the combination of HR and BR at which the changes in QRS and T wave morphology are statistically significantly different compared to a signal without breathing effects. We then evaluate the proportion of signal affected by BR, HR, and SNR in the PhysioNet Normal Sinus Rhythm data set to help elucidate the potential impact of these factors on MVM and TWA assessment.

2 Methods

The methods section is organized as follows. Section 2.1 describes the methods used to measure morphological variability in the QRS complex and the T waves. A standardized physiological model used for generating the data, used in evaluating the morphological variability at different HR's and BR's for statistical significance is described in section 2.2. The preprocessing applied to the data before performing the MVM and TWA analysis, like filtering out the noise, is described in section 2.3. Section 2.4 discusses the non-parametric surrogate-based test, which is used to determine when the changes in morphology detected due to BR and HR are statistically significantly different from a signal without breathing effects. Section 2.5 describes the testing methods, i.e., the ECG signals generated with different HR's, BR's, SNR's and morphologies are used to determine how morphological variability is affected by each of these factors.

2.1 Morphology analysis techniques

The methods included in this research, which capture morphology variations between successive QRS complexes, T waves or the entire beat on a beat by beat basis, are described below.

2.1.1 QRS complex

The QRS morphology variability technique is based on the method implemented by Liu *et al.* [4]. The first step of the QRS morphology analysis consists of isolating the QRS complexes in the signal by detecting the onset and offset times of each complex. Then, for each pair of adjacent beats, the QRS complexes are dynamically time-warped to align the shapes and be the same length. Time warping is performed using the DTW (Dynamic Time Warping) function in Matlab. The function stretches the 2 QRS complexes or T waves onto a common interval such that the sum of Euclidean distances between corresponding points is minimum. To stretch the QRS complexes, DTW repeats each element of either input as many times as necessary to achieve the minimum sum of Euclidean distances between corresponding points [27]. Dynamic time warping also causes the different points in the two complexes to align with respect to the underlying physiological phenomenon, i.e. peak systole aligns to peak systole. The sum of the squared difference is calculated between them, and this is repeated between successive QRS complexes over the entire five-minute window of data to create a squared difference (SD) series.

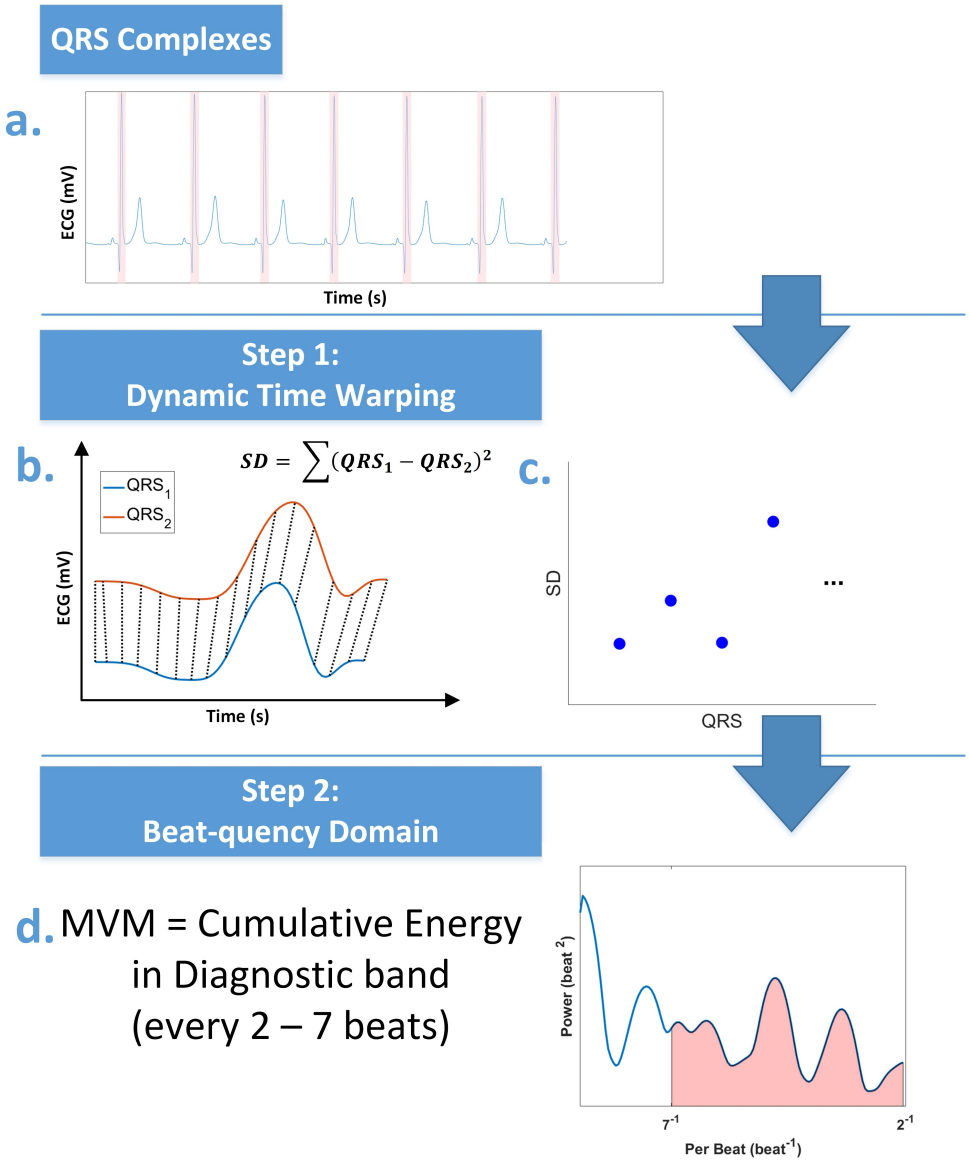

Figure 1: Illustration of the process for calculating MVM. a) The QRS complexes in each five-minute window of ECG are isolated. b) Dynamic time warping is performed between successive complexes and the sum of their squared difference is computed. c) These squared differences, SD series, are computed for the entire five-minute window and transformed to the beat-quency domain, analogous to the frequency domain, by applying the Fourier transform. d) The cumulative energy is measured in the range of every 2-7 heartbeats, as reported by [4].

Finally, the SD series is converted to the beat-quency domain [28].

As reported by Liu *et al.* [4], the morphological variation for heart patients is found to be highest in the every 2 to 7 beats region of the ECG before acute myocardial infarction. Accordingly, to the previous works, we measure the energy in the power spectrum (beat-quency domain) of the SD series in the range of every 2-7 heartbeats and label it the MVM. The methodology is summarized in figure 1.

2.1.2 T wave

We apply TWA detection based on [22]. It involves applying the MMA method for TWA detection and using a surrogate statistical test based on randomly reshuffling the T waves to determine the noise threshold. The noise threshold is used to determine when the TWA detection is not a false-positive detection. This algorithm is an established technique in literature and we intend to determine which HR and BR pairs cause false positive detection of TWA with varying SNR.

2.1.3 Entire beat

We evaluate MV over the entire ECG beat (MVB) as described by Liu *et al.* [4]. The methodology for evaluating MVB is similar to that described in figure 1. Instead of the QRS complexes, each ECG beat is isolated between successive R peaks in each 5-minute analysis window. Similar to before DTW is performed between successive beats before computing the SD series. The power spectrum is computed for the SD series and the cumulative energy is measured in the every 2 to 7 beat-quency band.

2.2 Data

In this work we use 3 ECG data sets which comprise 10 artificial 'subjects', 18 normal subjects and 195 subjects with or without post-traumatic stress disorder (PTSD), they are described below in the following 3 subsections.

2.2.1 Artificial ECG database

The methods are tested on artificial ECG signals generated using the simulator developed by Clifford *et al.* [29]. The simulator allows the generation of artificial ECG for a given HR, BR and morphology given a set of Gaussian coefficients. 12 lead ECG data, five minutes in duration, is generated with Lead I being used in the analysis. The generated ECG data has a sampling frequency (f_s) of 1 kHz and an amplitude resolution of 16-bits per sample, sufficiently high to limit quantization noise [30]. The high resolution of the ECG enables evaluating morphological variability on a finer scale.

A description of how the artificial ECG is generated is given as follows. A cardiac dipole vector in 3 dimensions is generated, $d(t) = x(t).\hat{a}_x + y(t).\hat{a}_y + z(t).\hat{a}_z$. The x, y and z are time-varying components in the 3 orthogonal directions. The orthogonal directions are aligned with the axes of the torso and the electrical activity is considered to be a vector cardiogram (VCG). The dynamics of the model are given in equation array 1,

$$\begin{aligned}
\dot{\theta} &= \omega, \\
\dot{x} &= -\sum_i \frac{\alpha_i^x \omega}{(b_i^x)^2} \Delta\theta_i^x \exp[-\frac{(\Delta\theta_i^x)^2}{2(b_i^2)^2}], \\
\dot{y} &= -\sum_i \frac{\alpha_i^y \omega}{(b_i^y)^2} \Delta\theta_i^y \exp[-\frac{(\Delta\theta_i^y)^2}{2(b_i^2)^2}], \\
\dot{z} &= -\sum_i \frac{\alpha_i^z \omega}{(b_i^z)^2} \Delta\theta_i^z \exp[-\frac{(\Delta\theta_i^z)^2}{2(b_i^2)^2}]
\end{aligned} \tag{1}$$

Where θ is the cardiac phase and sweeps between [-π,π] for each beat. ω (the rate of change of θ) depends on the instantaneous heart rate (bpm) for the current beat (h) and is computed as $\omega = 2\pi h/60$. The instantaneous heart rate is derived from the RR interval tachogram. The changes in the $\hat{a}_x$ direction can be written as a sum of Gaussian functions indexed with i and amplitude α_i^x, width b_i^x, located at rotational angle θ_i^x and $\Delta\theta_i^x = (\theta - \theta_i^x + \pi) \mathrm{mod}(2\pi) - \pi$. The rotational angle corresponds to when the Gaussian function peaks during the cardiac cycle. The intuition behind these equations is the variation along each orthogonal direction, assumed to be continuous functions, can be approximated arbitrarily well with a finite number of Gaussian functions [31]. The dipole vector coordinates, originally at a baseline or zero mV, are driven above or below the baseline as they approach the center of the Gaussian functions. This generates a variable length dipole vector that moves in three-dimensional (3D) space, forming the VCG signal along each of the orthogonal x, y and z axes. Moreover, small random deviations can be added to Gaussian parameters used for generating these vectors to simulate realistic ECG with inter-beat variability. Two forms of variability affecting the ECG beat are built into the model so it resembles realistic signals. First, dynamic heart rate variability (HRV), where the instantaneous heart rate for a given ECG signal can change bidirectionally with a standard deviation of 5 beats per minute (bpm) between consecutive beat intervals. Dynamic HRV results in QT interval variability in the simulated ECG [32, Fig. 10], where the QT interval is inversely related to the HR [33], [34].

Second, the breathing effect causes amplitude modulation of the QRS complex and T wave with a period determined by the HR and BR. In order to explain how breathing is added to the 12 lead artificial *ECG*, it can be decomposed as in equation 2,

$$ECG(t) = H.R.\Lambda.s(t) + w(t) \tag{2}$$

$s(t)$ is the VCG signal obtained from the cardiac dipole in 3D. $w(t)$ is additive noise. H is a $\mathbb{R}^{12\times3}$ matrix corresponding to the Dower transform to create 12 lead ECG from the VCG. Λ is a $\mathbb{R}^{3\times3}$ diagonal matrix used for scaling each VCG lead to the correct amplitude and R is a $\mathbb{R}^{3\times3}$ matrix that captures changes like the rotation of the dipole vector in 3D, similar to the breathing effect. H captures stationary information like body conductance and electrode locations.

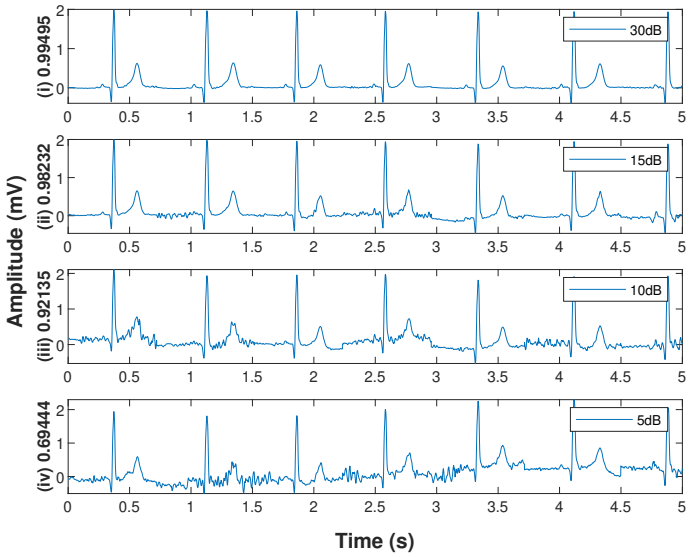

Figure 2: A five-second window of simulated ECG with SNRs of 30,15,10 and 5 dB is plotted in subplots (i), (ii), (iii) and (iv) respectively. The signal quality index for each signal is also given as the y-axis label for each plot. For each subplot, the y-axis is plotted as amplitude in mV. The x-axis is plotted as time in seconds.

R and Λ capture short term variation within the ECG and can vary with time. By varying the rotational angle for each lead in matrix R according to Givens rotation [35], corresponding periodic amplitude modulation of the ECG signal is introduced. The amplitude changes due to the breathing effect are added to each lead on a per sample basis. For more details on the generation of the artificial data, see appendix.

2.2.2 Normal Sinus Rhythm ECG database

We test our algorithm on data acquired from the Normal Sinus Rhythm (NSR) database on PhysioNet [36], [37]. The database contains two-channel ECG for each of 18 subjects sampled at 128 Hz. Each recording is approximately 24 hours in duration from healthy individuals, including 13 women, between the age of 20 and 50, and 5 men, between the age of 26 and 45.

2.2.3 Post-traumatic stress disorder ECG database

The PTSD database consists of 32 individuals with PTSD and 163 controls with no history of PTSD. Each individual has a 12 lead Holter ECG recording approximately 24 hours in duration. Increased levels of stress are reported to be correlated with increased MV of the ECG [38], [39], therefore we hypothesize PTSD individuals will have elevated MVB of the ECG compared to controls. We evaluate MVB, as described in section 2.1.3, for each individual in the PTSD database for each analyzable non-overlapping 5-minute window in each lead. For each individual, the 90^{th} percentile computed for the MVB measurements (MVB_{90}) in each lead, in addition to the HR and BR estimate for the corresponding window, is used as a feature to perform classification between the individuals with and without PTSD. We test the previously published MVB_{90} metric [4] to determine if adding HR and BR as features lead to an expected increase in classification performance.

2.3 Preprocessing

For each dataset in section 2.2, the baseline wander is removed from each signal using the median filter implemented by De Chazal *et al.* [40]. Two median filters, with orders $f_s/5$ and $3f_s/5$, are applied sequentially to estimate the baseline wander in the signal. The filter with order $f_s/5$ removes the QRS complexes and P waves and the filter with order $3f_s/5$ removes the T waves. The baseline wander estimate is then subtracted from the original signal. Following baseline wander removal, when evaluating MV on signals in the artificial ECG database, fiducial points are detected on the noise-free ECG signal with the wavelet-based algorithm developed by Martinez *et al.* [41] and used when evaluating MV on the ECG signal at different SNRs. When evaluating MV over the human ECG database, after baseline wander removal the signal is passed through a signal quality index (SQI) package [42] to ensure morphological changes measured are minimally affected by noise. The SQI algorithm uses two separate fiducial point detection algorithms, one noise sensitive and the other robust to noise. When the detected fiducial points for each agree, the signal is likely to be clean. Figure 2 illustrates how the SQI of the ECG signal drops as it becomes noisier. For the clean signals, fiducial points are detected by the automatic fiducial point detection algorithm developed by Martinez *et al.*

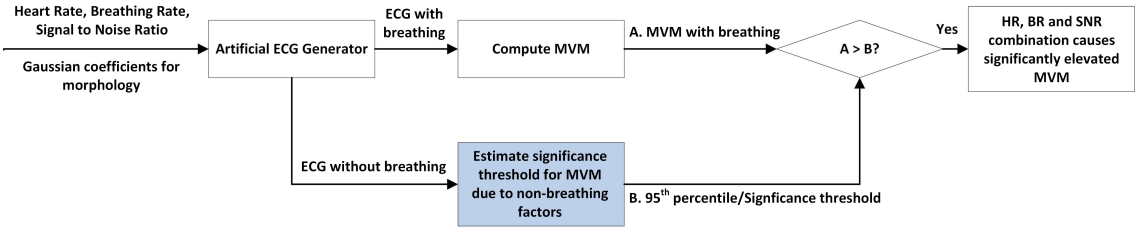

(A)

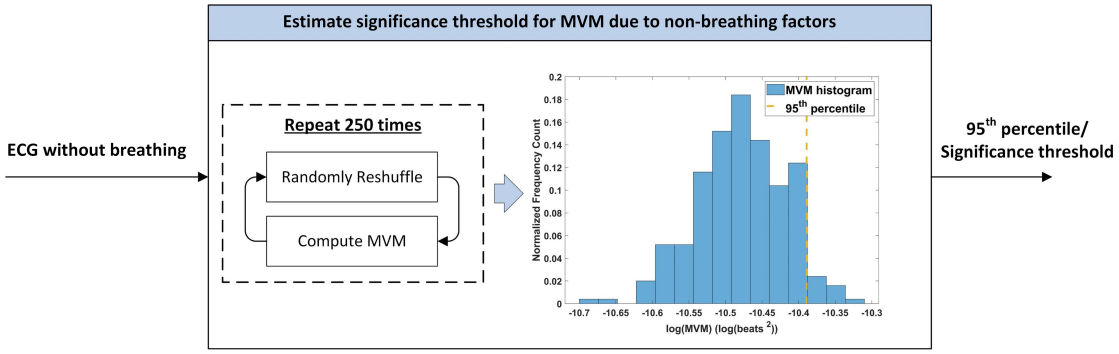

(B)

Figure 3: **A.** The flow diagram describes the procedure followed to determine if MVM measured from a signal with breathing is significantly elevated compared to a significance threshold estimated from a signal without breathing effect. **B.** The process given in the blue box in (A), of repeatedly reshuffling and estimating MVM to estimate the significance threshold is illustrated.

2.4 Statistical significance

MV due to the combined effect of HR and BR is measured in the ECG signal with breathing effect. To determine whether the MV measured is significantly elevated than normal, a significance threshold is determined from a similar ECG signal that does not have the breathing effect, but has other forms of variability like dynamic HRV and additive noise affecting the signal morphology.

We compute a non-parametric statistic described by Nemati *et al.* [22], to determine HR, BR and SNR combinations that lead to significantly elevated MV of the QRS complex and T wave when compared to MV measured in an artificial ECG without breathing effect. When evaluating the significance threshold for MVM, the QRS complexes in the ECG without breathing effect are randomly reshuffled and the cumulative energy is computed in the band of interest. This process of reshuffling and computing energy is repeated 250 times and the 95^{th} percentile of the energy measurements is considered to be the significance threshold. MVM measurements in the signal with breathing above this threshold are considered to be statistically significant with a p-value < 0.05. The process is summarized in figures 3A and 3B. For MVM evaluations the significance threshold is computed for a given heart rate. The signal with the breathing effect is not considered for estimating the significance threshold as a random reshuffling of the QRS complexes can cause MV energy due to breathing to spill into the beat-quency band of interest. We want to compare MV measured due to breathing to a significance threshold measured in the absence of breathing, as we look to determine conditions under which breathing driven changes will significantly elevate MV compared to MV measured in the absence of breathing effects.

TWA analysis is performed using the algorithm developed by Nemati *et al.* [22] and TWAs are considered significant at the 5% significance level. The T waves are reshuffled 250 times and the TWA amplitude estimate is computed after each reshuffle. A gamma distribution is fitted to the TWA amplitude estimations and the 95^{th} percentile of the fitted distribution is considered to be the significance threshold. The significance threshold is estimated from the signal with breathing. When estimating the significance threshold, the TWA significance test reshuffles the T waves in the original sequence to effectively remove any oscillatory behavior, except that likely by pure chance. If we repeat this 100 times and observe less than 5 sequences with higher or equivalent MV as the original sequence, then we can say that the likelihood of observing a true event is 4%, or significant at $p < 0.05$. Since the reshuffled sequence is constructed from the original data, it preserves all statistics except temporal correlations, providing an accurate non-parametric earmarked for the distribution of the noise at any given moment. Therefore, estimating the significance threshold for TWA from a separate breathing free signal is not needed.

2.5 Overview of testing methods

Section 2.5.1 describes how the TWA and MVM evaluation algorithms are verified to correctly measure MV. The verification is performed using typical artificial ECG generated using the simulator described in section 2.2.1. The simulator is used to generate ECG data with known MV of QRS complexes and T waves. The algorithms are used to determine how accurately this known variation can be estimated. Section 2.5.2 explains how the morphological variability measurement algorithm is applied to the artificial ECG database to determine HR and BR combinations, at a given SNR, that lead to elevated MV of the QRS complex and T wave. Once HR, BR and SNR combinations that lead to artificially inflated MV have been determined, MV is evaluated in the NSR ECG database. The fraction of analyzed windows with elevated MVM and TWA due to the combined effects of HR and BR is computed. The fraction of windows with TWAs above a critical threshold of 47 μV is computed, before and after accounting for analysis windows expected to have elevated MV due to HR and BR. The procedure is explained in section 2.5.3. The methods used to evaluate the classification between individuals with and without PTSD using MVB_{90}, HR and BR are described in detail in section 2.5.4.

2.5.1 Verification of the morphological variability algorithms

The TWA detection is performed using the MMA method, an established method in literature [43], coupled with the surrogate statistical test for noise rejection [22]. We verify the algorithm's accuracy by evaluating TWA on typical noise-free artificial ECG signals of five-minute duration, HR of 80 bpm, without breathing effect and known TWA amplitudes of 10, 20, 30, 40 and 50 μV [29]. For each signal, the TWAs are evaluated over 60 beat windows with 50% overlap and the estimated mean significant TWA amplitudes measured over the windows are 10.88, 20.19, 30.79, 40.34, 50.12 μVs. The estimated TWA amplitudes are close to the known TWA amplitudes. Similarly, typical artificial ECG is generated for HRs in the range 40,60,...,120 bpm in increments of 20, BRs in the range 0,4,6,9,...,30 rpm in increments of 3 and SNRs of 5,10,15 and 30 dB. For given HR, BR and SNR, the MVM is measured in a narrow band around the dominant beat-quency for the signal with and without breathing effect. The dominant beat-quency corresponds to the period of amplitude modulation of the ECG beats due to the breathing effect and is calculated as the ratio BR/HR. For a SNR of 30 dB, the MVM energy measured in the dominant beat-quency band is significantly higher in the signal with breathing than without breathing. As the SNR drops the difference in measured energy between the signal with and without breathing drops also. Due to the effects of noise, at 10 dB and lower the significance threshold measured from the signal without breathing exceeds the MVM energy measured from the signal with breathing for several HRs and BRs. Thus, it is verified the known MV of the T wave and QRS complex is accurately measured using the MV algorithms.

2.5.2 Effect of breathing rate, heart rate and noise on morphological variability in artificial data

This experiment aims to study how HR and BR combinations affect the statistically significant elevation of MV observed in each ECG morphology in the artificial ECG database, at different levels of SNR. The generation of the artificial ECG database is described in section 2.2.1. For each ECG morphology in the artificial ECG database, a signal is generated with HR varying from 40 to 120 bpm in 20 bpm increments and breathing rate varying as 0, 4 and 6 - 30 rpm, in increments of 3. The breathing rate of 0 refers to the signal without a breathing effect. The MV of the QRS complex and T wave in the breathing free signal is due to dynamic HRV and additive noise. When analyzing HR, BR and SNR combinations for effects on falsely elevated MVM, the energy in the signal with breathing is measured in a narrow band around the dominant beat-quency and is referred to as MVM_{nb}. The dominant beat-quency is calculated as BR/HR, section 2.5.1. For a HR of 80 bpm and a BR of 20 rpm, the dominant beat-quency is 0.25 $beats^{-1}$. If the beat-quency aliases, as is the case for HR 40 bpm and BR 30 rpm, the energy is measured in the energy band around the aliased beat-quency, in this case, 0.25 $beats^{-1}$. The significance threshold for the measured MVM_{nb} is estimated from the breathing free signal using the surrogate statistical test and is measured over the narrow band used for evaluating MVM_{nb}. This is discussed in section 2.4.

For each of the 10 morphologies in the artificial ECG database, MVM_{nb} is computed for the set of HR and BR combinations mentioned above and compared with the corresponding significance threshold. The fraction of morphologies that have MVM_{nb} above the corresponding significance threshold is computed for the specified range of HR and BR combinations at SNRs of 10, 15 and 30 dB. This fraction of morphologies with significantly elevated MVM_{nb} are presented as contour plots for HR vs BR for a given SNR in section 3.1. The results are used to determine the HR, BR and SNR combinations expected to cause significantly elevated MVM_{nb}, resulting in falsely elevated MVM for a large sample of individuals.

Similar to MVM, the set of HR, BR and SNR combinations that result in false-positive TWA detection are studied for each ECG morphology in the artificial ECG database. TWA analysis is performed in 60 beat windows with a 50% overlap. The number of overlapping 60 beat windows in a five-minute ECG is dependent on HR. Therefore the number of windows with significant detection is divided by the total

number of windows analyzed. We call this the false detection rate (FDR) and consider it our detection statistic for falsely elevated TWA at a given HR, BR and SNR. The FDR is averaged across the signals in the artificial ECG database for HR and BR ranges previously specified and presented as a filled contour plot for each SNR in section 3.2.

2.5.3 Effect of breathing rate, heart rate and noise on morphological variability in the Normal Sinus Rhythm database

We use channel 1 of ECG for each subject in our analysis. ECG data for each subject is upsampled to 1 kHz before analysis. For MVM analysis, non-overlapping five-minute windows in the ECG with a high SQI value are considered for analysis. Analyzing windows with a high SQI avoids measuring any erroneously elevated MVM due to noise. For TWAs, detection is considered significant after computing the non-parametric statistic, described in section 2.4. The significance threshold estimated by the non-parametric statistic is adaptive with respect to the level of noise in the ECG. A noisy ECG leads to estimating a higher significance threshold, reducing the chance for a significant TWA detection. As mentioned in section 2.4, TWAs evaluated on the NSR ECG database are considered to be significant at a 5% significance level. To accurately estimate the distribution of noise at any instant for MVM using the non-parametric statistic, the QRS complexes' sequence needs to be reshuffled to remove any oscillatory behavior and temporal correlations except those likely due to random chance. The sequence of QRS complexes needs to be reshuffled to prevent oscillatory behavior in the original sequence in every 2-7 beat band from reappearing in the every 2-7 beat band after reshuffling. The application of the non-parametric statistic for MVM is more involved than for TWAs, which measure variability in the T wave strictly over a period of two beats. It is to be noted the SQI is considered a standard for rejecting noisy ECG analysis windows. Previous works that use SQI to reject noisy ECG windows in their MV analysis include Liu *et al.* [4]. For TWAs, the analysis is conducted on windows with HRs below 120 bpm since TWAs measured at high heart rates can also be falsely detected due to the effects of breathing. For MVM and TWA analysis, the fraction of analyzed windows with MV significantly affected by HR and BR is computed. Since windows with high SQI are analyzed, the HR and BR combinations causing elevated MV at a SNR of 30 dB, enclosed by the white dotted contour in figures 4A and 5A, are used for determining the affected windows. The BR in each analysis window is estimated using open-source software by Charlton *et al.* [44]. The following method, which is reported as measuring breathing rate most accurately from the ECG is used. Specifically, the breathing signal is estimated in each analysis window from the variation in baseline, amplitude, and frequency of the ECG (mean amplitude of Q point and proceeding R-peak, R-peak amplitude and RR interval time series) [44]. For each of these three estimated breathing activity sources, the breathing rate is determined using the 'Count-Orig' method described by Schafer *et al.* [45], explained as follows. Each breathing signal estimate is bandpass filtered with a 10th order Butterworth filter, with a passband of 0.1 - 0.5 Hz. The local maxima and minima are then determined in this filtered signal. A threshold level is defined as 0.2 x 75th percentile of all maxima ordinate values. Each breathing cycle is considered to have begun and ended at consecutive local maxima above this threshold level. A breathing cycle is considered valid if there is only one minimum below zero and no other extrema between the maxima initiating and terminating the breathing cycle. The breathing frequency is estimated from the reciprocal of the average length (in seconds) of all valid breathing cycles. Each breathing rate estimate from each of the three sources (baseline, R-peak amplitude and RR interval time series) is fused using an averaging approach per Karlen *et al.* [46] to obtain a breathing rate estimate for the analysis windows. The HR is computed as the reciprocal of the median R peak to R peak interval in seconds in each analysis window divided by 60. For TWA analysis, the fraction of analyzed windows above a 'critical' threshold is reported, before and after correcting the effects of HR and BR. The corrected fraction of analyzed windows is computed by discarding data windows with TWA significantly affected due to HR and BR - see figure 5A. Following Verrier *et al.* [47], we choose a critical threshold of 47 μV. This allows us to demonstrate how TWA measurements may be falsely detected at elevated levels associated with poor health outcomes when impacted by these factors. We note that the removal of windows with MV inflated due to HR and BR is indeed a novel approach.

2.5.4 Effect of breathing rate, heart rate and noise on morphological variability in the PTSD database

The MVB is measured for each non-overlapping 5-minute window, determined to be analyzable using the SQI algorithm, in each lead. For each lead, the MVB value closest to MVB_{90} is considered as a feature to classify individuals with and without PTSD. HR and BR are added as additional features and it is hypothesized adding these features will lead to an increase in the classification performance. HR is estimated as described in section 2.5.3. BR is estimated using the 'Count-Orig' method applied to the breathing signal estimated from the amplitude changes. The fused estimate is evaluated when the BR estimate from each amplitude, frequency and baseline variation is close. It is therefore missing in a few of the windows for which MVB_{90} is included as a feature. Ten-fold cross-validation (CV) with a logistic regression classifier is used to evaluate each feature set's performance.

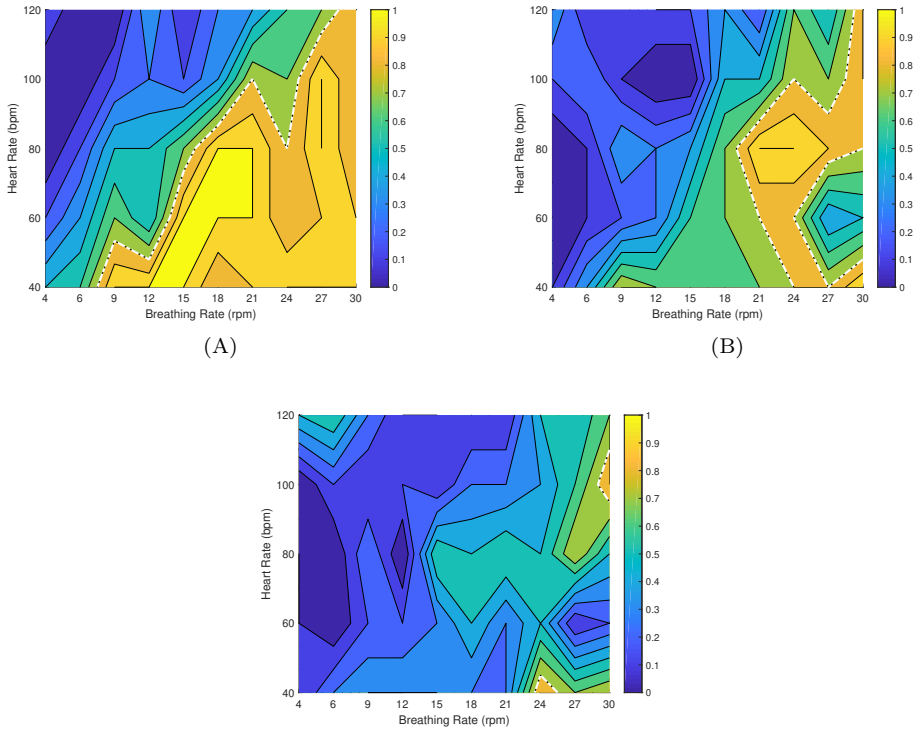

(A) (B)

(C)

Figure 4: For different HR, BR and SNR combinations, MVM_{nb}, section 2.5.2, is measured in each signal in the artificial ECG database. For each SNR, the fraction of 10 signals with significantly elevated MVM_{nb} compared to the corresponding significance threshold are plotted for HR versus BR. The white dotted contour encloses HR and BR combinations which cause significantly elevated MVM_{nb} in at least 8 of the 10 signals in the artificial ECG database. **A.** For a SNR of 30 dB, low HRs and high BRs result in significantly elevated MVM_{nb} for a large fraction of signals. **B.** For a SNR of 15 dB, HR/BR pairs in a healthy individual's physiological range, i.e. 60/15, 60/18, 80/18 and 80/20 bpm/rpm cause significantly elevated MVM_{nb} in at least 6 artificial ECGs. **C.** For a SNR of 10 dB, HR/BR pairs outside the physiological range of healthy individuals, i.e. 40/24 and 100/30 bpm/rpm, cause significantly elevated MVM_{nb} in a large fraction of signals.

Thirty-two control individuals are randomly sampled from the whole group of controls to create a balanced dataset of PTSD and control individuals for performing classification. The process of sampling controls and performing classification is repeated eight times, and the average area under the receiver operator characteristic curve (AUROC) is reported. The average AUROC is reported for classification performed using MVB_{90} separately and MVB_{90}, HR and BR combined. The distribution of AUROCs for classification with MVB_{90}, HR, BR is compared to that with MVB_{90} only. Classification is performed with the average HR and average BR for each individual to determine if the features are independently predictive of PTSD.

3 Results

The results section is organized as follows. Section 3.1 details the results for HR, BR and SNR combinations that lead to falsely elevated MVM in the artificial ECG database. Section 3.2 details the results for HR, BR and SNR combinations that lead to falsely elevated TWA detection in the artificial ECG database. Section 3.3.1 presents the results for MVM and TWA analysis on the NSR database, before and after correcting for the effects of HR and BR. Section 3.3.2 presents the results for classification performed on the PTSD database using MVB_{90}, HR and BR.

3.1 Effects of breathing rate, heart rate and noise on QRS morphological variability

Figures 4A - C show the filled contour plots for the fraction of signals in the artificial ECG database with MVM_{nb}, explained in section 2.5.2, above the corresponding significance threshold. For a given SNR, HR, and BR, the fraction of artificial ECGs with significantly elevated MVM_{nb} is 1 when all ten artificial ECGs have significantly elevated MVM_{nb} and 0 when none of the signals have significantly elevated MVM_{nb}

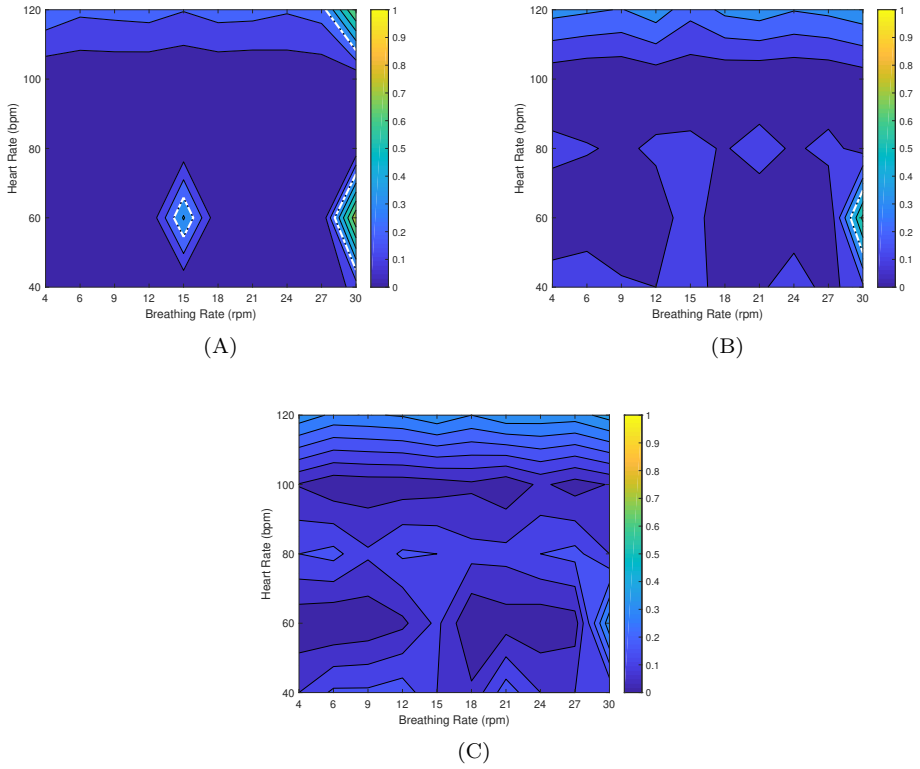

Figure 5: The FDR for TWA, explained in section 2.5.2, is computed for each signal in the artificial ECG database over a range of HR and BR combinations for a given SNR. The FDRs are averaged across the 10 signals for each SNR and presented as a filled contour plot for HR versus BR. **A.** The average FDR is measured at a SNR of 30 dB. Falsely elevated TWAs are observed for HR and BR pairs of 60/30 bpm/rpm, 120/30 bpm/rpm and 60/15 bpm/rpm. **B.** The average FDR is measured at a SNR of 15 dB. Falsely elevated TWAs are observed at the HR and BR pair of 60/30 bpm/rpm. **C.** The average FDR is measured at a SNR of 10 dB. Falsely elevated TWAs are not observed for any HR and BR pair suggesting the signal is too noisy for reliable TWA detection. In each figure, a white dotted contour encloses HR and BR combinations which falsely elevate TWA detection.

compared to the corresponding significance threshold. The SNR varies as 30, 15 and 10 dB in figures A to C. The white dotted contour encloses HR and BR combinations for which an abnormally large fraction, at least 8 of the 10 signals have MVM_{nb} above the corresponding significance threshold. At a SNR of 30 dB, a small fraction of signals have significantly elevated MVM_{nb} energy for high HRs and low BRs. The amplitude-modulated changes due to breathing are small between consecutive beats at high HR. They are comparable to general morphology changes between QRS complexes and hence are not significant. For a SNR of 30 dB, HRs between 60-80 bpm and BRs between 15-21 rpm cause significantly elevated MVM_{nb} in at least 8 of the artificial ECGs. These HR and BR combinations are common in healthy individuals. For a SNR of 15dB, for HRs between 60-80 bpm, BRs above 17 rpm cause falsely elevated MVM in at least six artificial ECGs. For a SNR of 10 dB, HR/BR pairs of 40/24 and 100/30 bpm/rpm cause falsely elevated MVM in at least eight artificial ECGs. However, these HR/BR pairs are outside the physiological range of healthy individuals.

3.2 Effects of breathing rate, heart rate and noise on T-Wave variability

For different SNRs, HR and BR combinations which falsely elevate TWA are determined. The FDR, explained in section 2.5.2, is computed over a range of HR and BR combinations for each signal in the artificial ECG database and averaged for each SNR. The averaged result is presented as a filled contour plot. For a given SNR, HR, and BR, the average FDR is 1 when all of the analyzed windows in each artificial ECG have a significant TWA detection and 0 when none of the signals have significant TWA detection in any analysis window. For a SNR of 30 dB, figure 5A, the false elevation of TWAs is observed at HR/BR pairs of 60/30 bpm/rpm, 60/15 bpm/rpm and 120/30 bpm/rpm. The HR/BR of 60/30 bpm/rpm is obvious as the breathing rate is exactly half the HR, which will induce T wave amplitude modulation with period 2. The HR/BR pair of 60/15 bpm/rpm is not as obvious. When the BR is $1/4^{th}$ the HR, the breathing cycle causes a difference in amplitude between the average even and average odd indexed T wave. This difference is detected by the MMA method used for TWA evaluation. This observation is

confirmed by the significant number of false elevations at a HR/BR pair of 120/30 bpm/rpm. For a SNR of 15 dB, figure 5B, there is false elevation of TWA observed at a HR/BR pair of 60/30 bpm/rpm. At a SNR of 10 dB, figure 5C, The signal is too noisy for reliable TWA detection. For each SNR, HR and BR combinations, which cause significant false TWA detection in at least 40% of all analyzed windows, are enclosed by the dotted white contour in the respective plot.

3.3 Effects of breathing rate and heart rate on morphological variability in real data

3.3.1 Normal Sinus Rhythm database

The fraction of MVM and TWA windows significantly affected by HR and BR are 66.76% and 8.33% respectively. The results suggest a significant part of the data has MV confounded by the effects of HR and BR; ignoring this data may lead to a bias. As noted in section 2.5.3, TWA presence and magnitude is estimated in analysis windows with HRs less than 120 bpm. The fraction of significant TWA amplitudes above 47 μV before and after adjusting for HR and BR are 1.75% and 1.34% respectively. The fraction drops after adjustment indicating HR and BR effects can falsely inflate TWA amplitudes to elevated levels associated with poor health outcomes. TWAs above a threshold of 47 μV are predictive of sudden cardiac death (SCD) [47].

3.3.2 PTSD database

The highest average AUROC, across leads, evaluated using MVB_{90} in lead II as a feature is 0.54, with PTSD individuals having higher MVB_{90} than controls in lead II. After adding the HR and BR estimated for each corresponding analysis window, the average AUROC increased to 0.60. The results suggest that adding HR and BR as additional parameters improves separation between the PTSD and control individuals, compared to when independently using MVB_{90} for classification. The distribution for eight repeated AUROCs evaluated using MVB_{90}, HR and BR is significantly higher than that evaluated using MVB_{90} only with a p-value < 0.05. The two-sample Kolmogorov-Smirnov test is used to determine a significant difference. Classification using the average HR and average BR yielded eight repeated average AUROCs of 0.53 and 0.48, suggesting both features are not predictive of PTSD.

4 Discussion

Our study shows, for the first time, the need to consider breathing rates in addition to heart rates and SNR when measuring MV. Other studies have used alternative methods to exclude confounding observations, (notably using high heart rate thresholds or statistical rejection techniques) but do not explicitly consider breathing. Nearing *et al.* measure MV in T waves in an alternating pattern and only exclude analyses at high heart rates [7]. Nemati *et al.* add a non-parametric statistical significance test to reduce the false positive detection based on noise, but this method does not consider breathing effects [22]. However, their work does consider the effect of heart rate on TWA and they notice a paradoxical rise in TWA during sleep / at low heart rates, which can be explained by the confounding effect of breathing [48]. Liu *et al.* measure MV of the entire ECG beat including the QRS complex and the T wave in a non-alternating pattern, and use a signal quality index (developed by Li and Clifford and published in [49], [50]) to reduce any false-positive detections of elevated MV due to noise [4]. Similar to other studies, they also ignore breathing effects, or rather, these are implicitly captured in the analysis and may even dominate the metric. Our work demonstrates significant effects on MV of ECG due to breathing (at specific HR's and SNR's) and therefore highlights an important gap in previous work, which may well have included false triggers related to breathing rate, heart rate and noise. Such covariance between HR, BR and condition/outcome often differs between populations and can lead to false conclusions, both positive and negative.

Our findings are consistent with previous literature that demonstrates alterations in QRS complex and T wave morphology with breathing [51] and heart rate variability [52]. These morphological changes in the QRS complex and T wave correlate with those in MVM and TWA, respectively. Breathing causes changes in chest impedance and the position of the heart with respect to the ECG electrodes, both of which lead to amplitude modulation of the QRS complex and T wave [53]. Moody *et al.* build upon these principles and estimate the breathing signal from QRS complex amplitude modulations due to breathing [51]. For TWA, false positives are observed when the ratio of the heart rate and breathing rate is a factor of 2. For these heart rate and breathing rate pairs, the T wave amplitudes are modulated so that there is a significant difference in amplitude between average even and average odd indexed beats being analyzed. It is important to note these HR and BR combinations will not necessarily cause false positive detection for other TWA detection algorithms. For example, the spectral method [47] will only detect falsely elevated TWAs at HR to BR ratios of 2, since variability with periods 4, 8, ... are measured at the separate frequency intervals 0.25, 0.125, ... Hz respectively. Increased false-positive detection of MVM is

detected for low heart rates and high breathing rates. Under these conditions, there is higher beat-to-beat variability measured in the beat-quency domain. Situations in which false-positive elevations occur are plausible. As shown in figures 4A and 4B, many elevations in MVM occurred at breathing rates and heart rates that are considered physiologically normal, including 12-20 rpm and 60-80 bpm. For TWA, breathing rate and heart rate pairs of 15 rpm and 60 bpm or 20 rpm and 80 bpm are likely a common occurrence. There is a greater confounding effect in MV observed at high values of SNRs for both QRS complexes and T waves, figure 4 and figure 5 respectively. The confounding effect of heart rate and breathing rate are observable in MV for SNRs above 15 dB. For lower values of SNR, the effects of breathing are less apparent. Nonetheless, these signals are more likely excluded from analysis because of poor quality.

These findings are subject to certain limitations. First, our findings are based on simulated ECG data and normal patients. Although this may be thought of as a limitation, it is a necessary step in defining a ground truth and produces an extensive analysis. Experiments are performed on realistic simulated ECG with dynamic heart rate variability and breathing effect built into the model. Notably, the ECG morphologies are derived from signals in the PTBDB on PhysioNet. These signals are considered to be the gold standard, to determine conditions of HR and BR expected to cause false-positive detection of MV on a larger sample size. We perform the analysis for different SNRs to determine how noise affects the rate of false-positive detection. We also note that experiments are then performed on real data from the NSR database, and the existence of 'natural' T Wave Alternans is significantly reduced in this normal population, casting doubt on the notion of such non-pathological variability. A follow-up study will analyze ECG data obtained from a large population of cardiac patients, approximately 1000, in a principled way to investigate the effects of heart rate and breathing rate on MV, and as independent predictors.

Future studies need to consider adjusting for breathing rate and heart rate when measuring MV. Currently, when evaluating TWAs, MV measurements are corrected by removing windows significantly affected by HR and BR, thus resulting in data loss that may cause a bias itself.

Possible mitigation strategies include a simple approach to correct MV measurements for BR and HR, similar to QT interval correction for heart rate [54]. Simulations can be used to determine the relationship between BR, HR, breathing signal amplitude and the MV measurements. The MV measurements expected due to breathing rate and heart rate effects can be subtracted from the MV measurements made from the actual ECG signal being analyzed. This approach is somewhat ad hoc, though. A more principled, but data-intensive approach could be to measure the breathing rate and heart rate in ECG windows and present them to the prediction model (with the MVM and TWA measurements) as independent parameters at the time of training. In this way, the model will learn to adjust the decision boundary for the effect of BR and HR on non-pathologically elevated TWA and MVM, for a given population.

To investigate the effect of HR and BR as features in addition to MVB, a cohort of individuals with and without PTSD is analyzed. The addition of HR and BR to MVB_{90} as features for classifying PTSD individuals from controls results in a 6% increase in average classification AUROC. Although the database's size is limited, with only 32 individuals with PTSD, the results encourage and motivate investigation on a larger balanced database with a higher number of patients. Both average HR and BR independently are not predictive of PTSD.

The study aims to improve methods for calculation of MVM and TWA by closely examining the extent to which breathing rate coupled with heart rate and noise may artifactually inflate results and falsely indicate increased arrhythmic risk due to cardiovascular disease. By doing so, we may underscore the importance of evaluating breathing separately and recognize its potentially independent effects in classifying arrhythmia risk. This is particularly important when considering interventions focused on the heart versus lungs, for example. To facilitate further examination of this paradigm, we also provide an open-source toolbox that has been stress tested to accurately measure morphological variability in realistic simulated ECG under varying amounts of noise. This toolbox will allow others to repeat the work presented here and examine new data for the confounding factors of heart rate and breathing rate [49], [50].

5 Conclusion

In this experimental study of synthesized ECG comparing MVM and TWA at varying heart rates, breathing rates, and SNR's using synthetic ECG data, we find a strong confounding influence at high breathing rates and low heart rates that likely inflate the conventionally measured results. In real data tests in normal individuals in which little variability due to cardiovascular disease (CVD) is expected, 67% and 8% of the ECG signal showed elevations in MVM and TWA respectively, due to these effects. These results suggest misclassification due to non-cardiac effects, especially for MVM. Future algorithms need to consider these effects as independent variables when attempting to accurately measure TWA and MVM in the context of CVD or other conditions, rather than the indirect influence of BR, HR, and SNR on MV.

Acknowledgments

The authors wish to acknowledge the National Science Foundation (NSF) award #1636933 "BD Spokes: SPOKE: SOUTH: Large-Scale Medical Informatics for Patient Care Coordination and Engagement", and National Institutes of Health/National Heart, Lung, and Blood Institute (awards R01HL136205, K23HL127251 and R03HL146879).

Any opinions, findings, and conclusions or recommendations expressed in this material are those of the authors and do not necessarily reflect the views of the sponsors.

Appendix. Generation of artificial ECG data

The rotational angle for lead X, $\Phi_x(n)$ is varied according to equation array 3.

$$\begin{aligned}
\Phi_x(n) &= \sum_{p=0}^{\inf} \zeta_x \frac{1}{1+\exp^{-\lambda_i(p)(n-\kappa_i(p))}} \frac{1}{1+\exp^{\lambda_e(p)(n-\kappa_e(p))}}, \\
\lambda_i(p) &= 20\frac{f_r(p)}{f_s}, \kappa_i(p) = \kappa_i(p-1) + \frac{f_s}{f_r(p-1)}, \kappa_i(0) = 0.35 f_s, \\
\lambda_e(p) &= 15\frac{f_r(p)}{f_s}, \kappa_e(p) = \kappa_e(p-1) + \frac{f_s}{f_r(p-1)}, \kappa_e(0) = 0.6 f_s,
\end{aligned} \tag{3}$$

where n denotes the sample index, p the breathing cycle index, $1/\lambda_i(p)$ and $1/\lambda_e(p)$ are the duration for inhalation and exhalation periods respectively, $\kappa_i(p)$ and $\kappa_e(p)$ are the delays for the inhalation and exhalation in the sigmoidal functions for breathing cycle p, f_s is the sampling rate, $f_r(p)$ the breathing frequency in breaths per second and ζ_x the maximum angular variation for lead X, which is set to 9 degrees. Φ_x(n) is ζ_x times the summation over each breathing cycle, of the product of 2 sigmoidal functions, one for inhalation and exhalation each. Due to the behaviour of the product of the sigmoidal functions, the angle $\Phi_x(n)$ changes with the sample number. It starts from zero, rises to the maximum value at peak inhalation and drops back towards zero near peak exhalation in each cardiac cycle. The same procedure is applied for the rotation of leads Y and Z, $\zeta_y = \zeta_z = \zeta_x$. Adding the breathing effect in this manner results in realistic amplitude variations in each lead, observed as variation in QRS area and RS amplitude [55]. The ECG is generated according to equation 2. The methodology for the artificial ECG generation is explained in further detail in the original works by McSharry *et al.* [32], Sameni *et al.* [35] and Clifford *et al.* [29].

The ECG simulator also has been shown to accurately generate abnormalities such as TWAs of varying amplitudes [29]. By slightly increasing the amplitude of the Gaussian functions with index $i = 9$, 10 and 11 in equation array 1 for every other beat, the affected T waves are generated with a slightly larger amplitude and artificial ECG with TWAs can be generated. The code for the ECG simulator is provided as part of the open-source toolbox. Additionally, external recorded noise available in the noise stress test database (NSTDB) [56] on PhysioNet is added to the generated ECG. The NSTDB comprises three types of noise, i.e. baseline wander, electrode movement and muscle artifacts. A five-second window of a simulated ECG with a HR of 80 bpm, BR of 10 respirations per minute (rpm) and TWA amplitude of 28 μV is plotted in figure A1.A. Figures A1.B and A1.C show an enlarged view of how breathing affects the amplitude of the QRS complex and T wave. The morphological variability analysis algorithms measure variations due to the periodic modulation of the ECG beat amplitude and compare them with changes measured in the absence of breathing affects, at the same heart rate to determine statistically significant differences.

To improve the generalization of our results, 10 ECG signals with different morphologies are generated. The QRS complexes and T waves have different R peak amplitudes, Q point, S point amplitudes, T peak amplitudes and shape / QRS axis. Following Clifford and McSharry [32] and Nemati *et al.* [22], the morphologies are derived from a variety of example beats so that the effects of HR and BR leading to elevated MV estimates are considered over a broad range of potential morphologies. These morphologies are derived using a least-square fit of Gaussian parameters (in the VCG representation) to subjects in the Physikalisch-Technische Bundesanstalt database (PTBDB) [57]. The ECGBeatFitter algorithm, found in [58], is used for deriving the least-square fit of Gaussian parameters to the VCG. The Dower transform is then applied to map these beats into the 12-lead representation. Hereafter these 10 ECG morphologies will be referred to as the 'artificial ECG database'. Five-second windows for each artificial VCG, figures A2 - A11, and the Gaussian parameters used for generating the VCG signals, tables A1 and A2, can be found in the appendix. For each of these 10 signals, different HR and BR combinations are analyzed to determine when significant elevations in morphological variability of the QRS complex and T wave are observed. The process is repeated for different SNRs to determine at which noise levels the changes observed remain significantly elevated. Conditions of SNR, HR and BR which lead to significantly elevated MV in a large fraction of the artificial ECG database, are expected to lead to falsely elevated MV in a larger sample population. Details on testing methods are discussed in section 2.5.

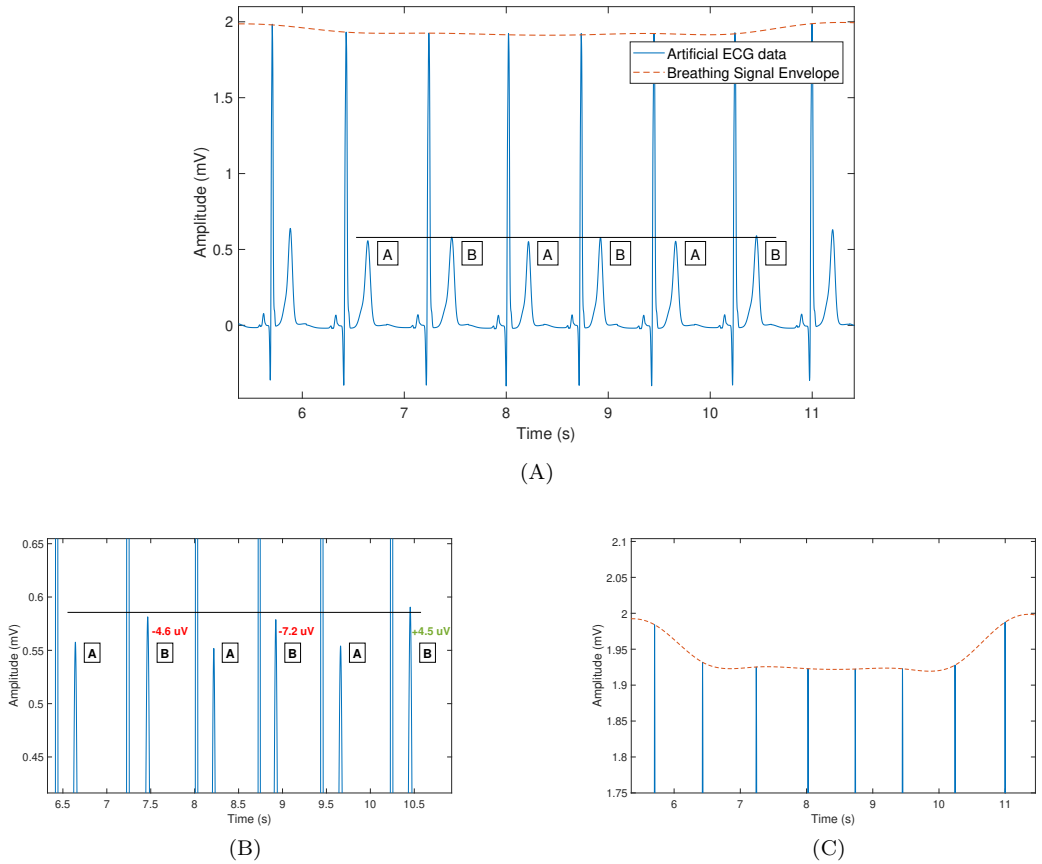

(A)

(B)

(C)

Figure A1: **A.** A five-second window of simulated ECG at HR 80 bpm, breathing rate of 10 rpm and T wave alternan amplitude of 28 μV is plotted. The T waves are assigned to group A or B, depending on the beat index. A horizontal line corresponding to the higher amplitude of T waves in group B in the absence of breathing is drawn, so the TWAs are clearly observed. The envelope of the QRS complex amplitudes corresponding to the breathing signal is marked with a dashed line. **B.** An enlarged view of the T wave peaks is shown. Breathing modulates the T wave amplitude causing it to rise above or below the indicated level. For T waves in group B, the change in amplitude caused by the breathing effect is shown in red if it drops below the given level and green if it rises above the level during exhalation. **C.** An enlarged view of the envelope of the QRS complexes amplitude is shown. The effects of breathing are apparent in the modulation of the QRS complex and T wave amplitude.

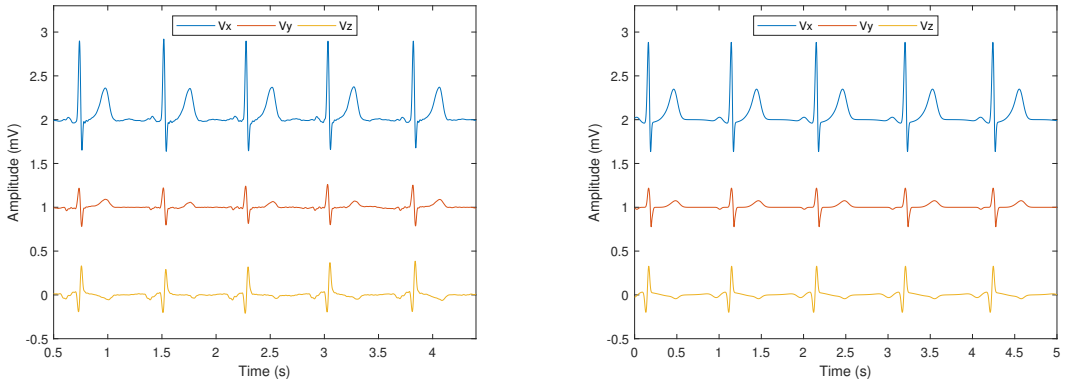

(A) (B)

Figure A2: (A) A five-beat window of the original VCG for recording s0303lre from patient 105 in the PTBDB. (B) The same VCG approximated using Gaussians.

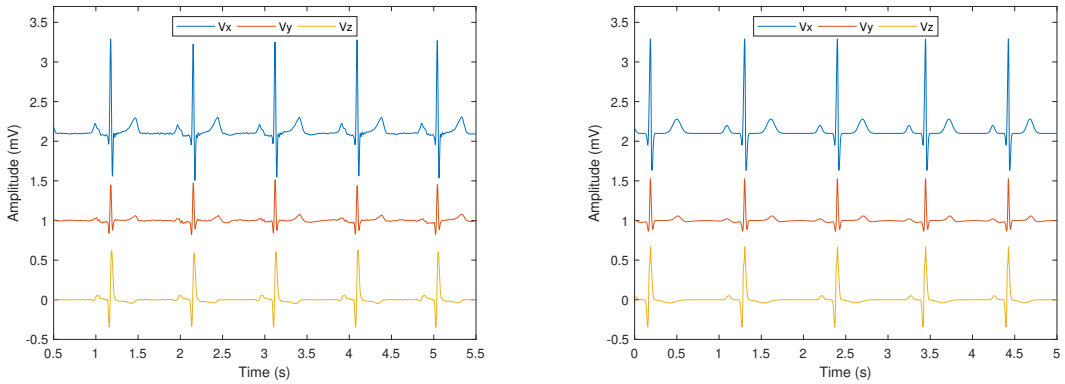

(A) (B)

Figure A3: (A) A five-beat window of the original VCG for recording s0302lre from patient 116 in the PTBDB. (B) The same VCG approximated using Gaussians.

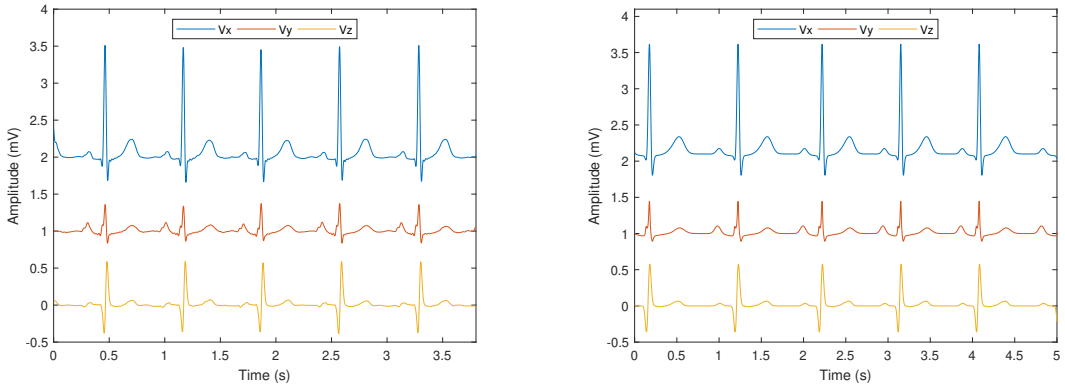

(A) (B)

Figure A4: (A) A five-beat window of the original VCG for recording s0311lre from patient 121 in the PTBDB. (B) The same VCG approximated using Gaussians.

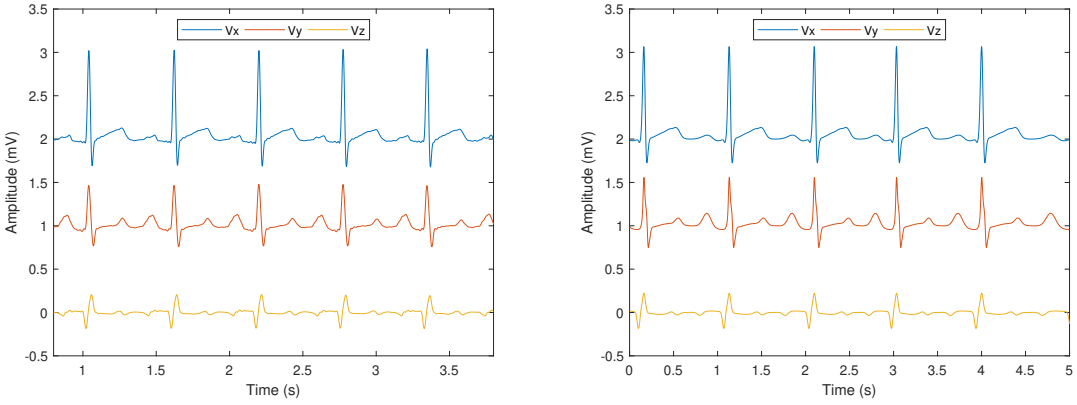

(A) (B)

Figure A5: (A) A five-beat window of the original VCG for recording s0273lre from patient 131 in the PTBDB. (B) The same VCG approximated using Gaussians.

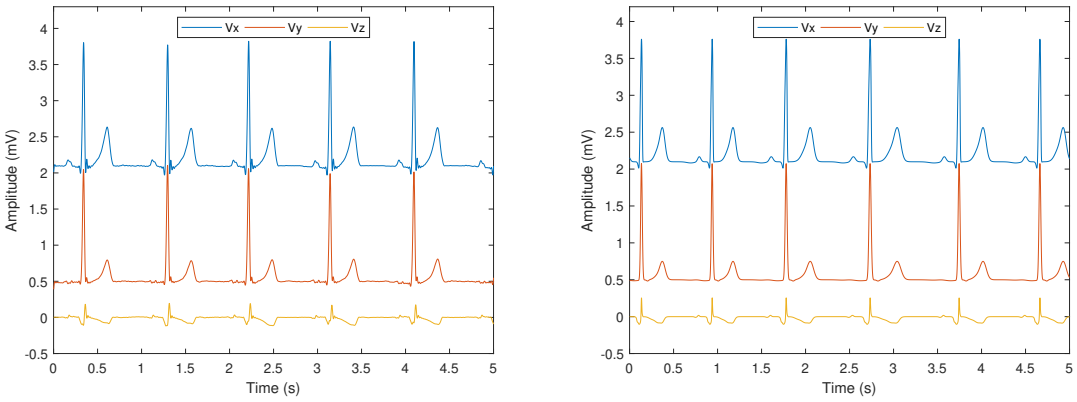

(A) (B)

Figure A6: (A) A five-beat window of the original VCG for recording s0287lre from patient 150 in the PTBDB. (B) The same VCG approximated using Gaussians.

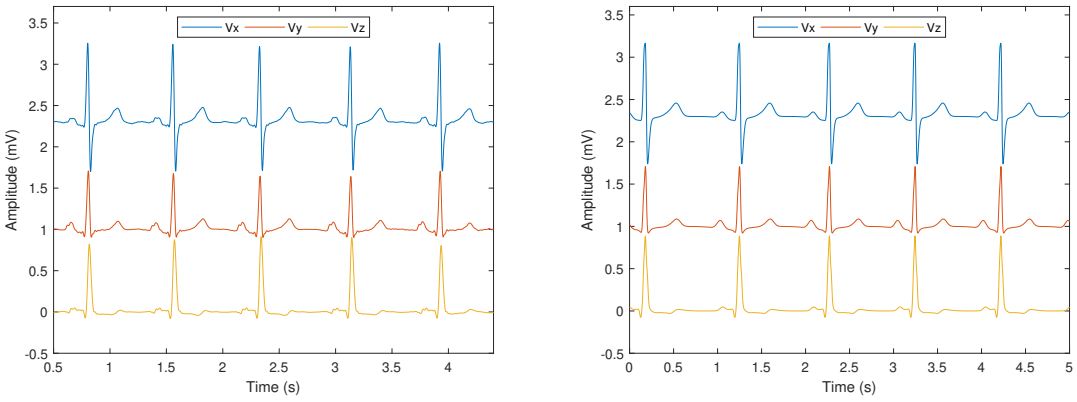

(A) (B)

Figure A7: (A) A five-beat window of the original VCG for recording s0301lre from patient 155 in the PTBDB. (B) The same VCG approximated using Gaussians.

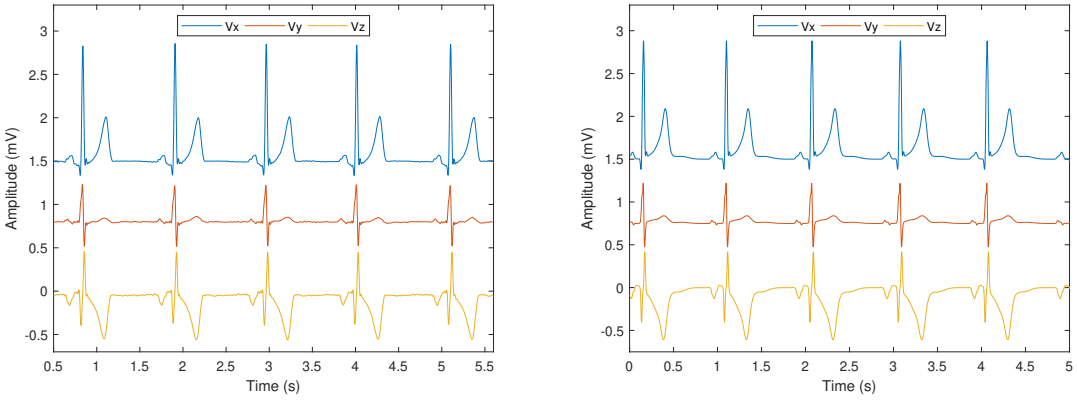

(A) (B)

Figure A8: (A) A five-beat window of the original VCG for recording s0323lre from patient 165 in the PTBDB. (B) The same VCG approximated using Gaussians.

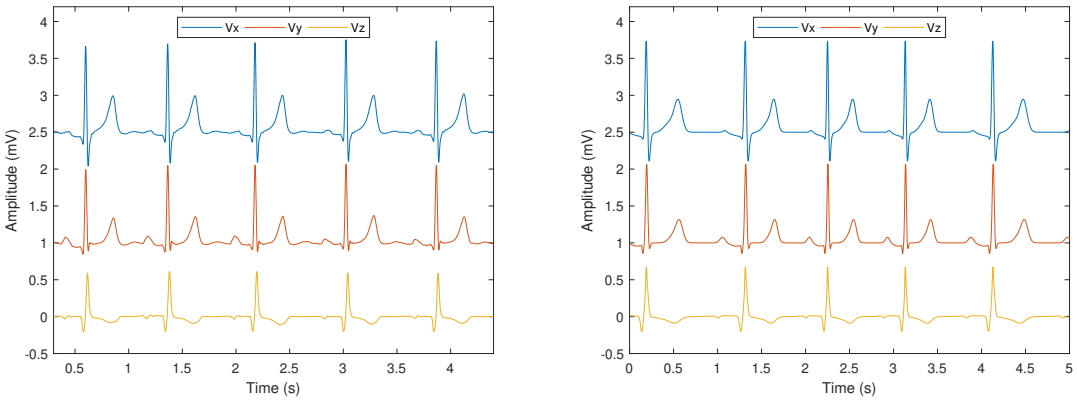

(A) (B)

Figure A9: (A) A five-beat window of the original VCG for recording s0300lre from patient 174 in the PTBDB. (B) The same VCG approximated using Gaussians.

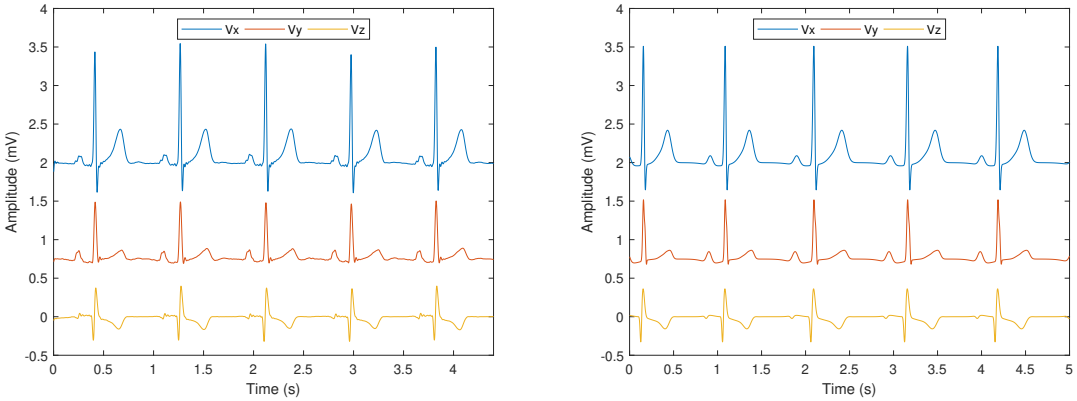

(A) (B)

Figure A10: (A) A five-beat window of the original VCG recording for s0308lre from patient 182 in the PTBDB. (B) The same VCG approximated using Gaussians.

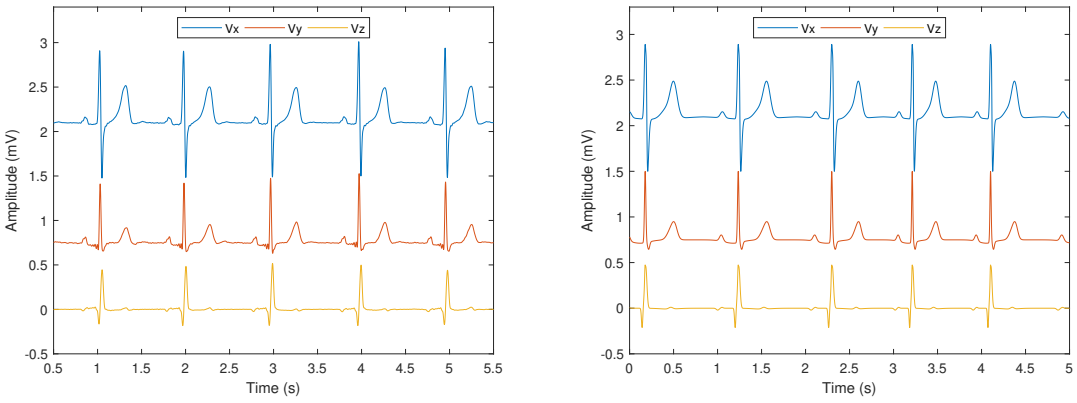

(A) (B)

Figure A11: (A) A five-beat window of the original VCG for recording s0336lre from patient 185 in the PTBDB. (B) The same VCG approximated using Gaussians.

Record #	Index (i)	1	2	3	4	5	6	7	8	9	10
patient105/s0303lre	α_i^x	-0.04	0.06	0.98	-0.60	0.10	0.29				
	b_i^x	0.78	0.23	0.09	-0.06	0.37	0.26				
	θ_i^x	-0.32	-0.88	0.001	0.13	1.55	1.95				
	α_i^y	0.22	-0.16	-0.11	-0.02	0.04	0.05				
	b_i^y	0.08	0.04	-0.07	0.11	-0.31	0.25				
	θ_i^y	0.005	0.18	0.25	-0.88	1.81	2.13				
	α_i^z	0.31	-0.24	0.04	-0.06	-0.02	-0.03				
	b_i^z	0.07	0.08	0.95	0.28	0.51	0.21				
	θ_i^z	0.01	-0.20	-0.56	-1.13	1.58	2.08				
patient116/s0302lre	α_i^x	2.50	1.38	-0.32	0.18	0.10	-1.83				
	b_i^x	0.05	0.05	0.02	0.26	0.15	0.09				
	θ_i^x	0.01	-0.07	0.07	1.76	-1.19	-0.01				
	α_i^y	-0.19	0.22	0.16	0.10	0.04	0.07	2.22	-1.90		
	b_i^y	0.93	0.03	0.61	0.54	0.20	0.21	0.08	0.09		
	θ_i^y	0.57	-0.01	0.26	1.25	-1.16	1.85	0.01	0.01		
	α_i^z	0.57	-0.44	0.05	-0.04	0.28	0.12				
	b_i^z	0.09	0.07	0.13	0.41	0.03	0.02				
	θ_i^z	-0.004	-0.16	-1.07	1.27	-0.09	0.005				
patient121/s0311lre	α_i^x	3.94	-0.03	-2.43	0.15	0.12	0.08				
	b_i^x	0.10	-0.73	0.12	0.31	0.40	0.20				
	θ_i^x	0.00	-0.05	0.02	2.19	1.85	-1.34				
	α_i^y	0.20	0.08	0.23	-0.04	0.11	0.08	0.17	0.17	-0.23	
	b_i^y	0.03	0.04	0.04	-0.67	0.21	0.35	0.07	0.14	0.10	
	θ_i^y	0.01	-0.24	-0.03	-0.07	-1.46	2.13	0.08	-0.03	0.10	
	α_i^z	1.07	-1.00	-0.01	0.05	0.04	0.04				
	b_i^z	0.12	0.11	0.18	0.28	0.18	0.18				
	θ_i^z	-0.05	-0.14	0.77	1.83	2.15	-1.30				
patient131/s0273lre	α_i^x	1.46	-0.05	-0.62	0.08	0.21	0.06	-0.12	-0.04		
	b_i^x	0.10	-0.32	-0.12	0.54	0.30	0.46	0.22	0.07		
	θ_i^x	0.01	-1.00	0.11	1.51	2.23	-1.43	2.17	-0.32		
	α_i^y	0.35	-0.04	-0.14	0.03	0.07	0.16	-0.23	0.28		
	b_i^y	0.05	0.85	0.08	0.62	0.22	0.30	0.05	0.15		
	θ_i^y	-0.01	-0.42	0.40	1.88	2.53	-1.65	0.30	0.07		
	α_i^z	-0.19	0.22	-0.02	0.03	0.02	0.02	-0.04	-0.03		
	b_i^z	0.10	0.11	-0.64	0.05	0.66	0.19	0.19	0.19		
	θ_i^z	-0.40	-0.003	1.20	-0.22	-1.34	2.05	-2.16	2.42		
patient150/s0287lre	α_i^x	1.14	1.14	0.20	0.64	0.33	-0.02	0.07	-0.20		
	b_i^x	0.04	0.06	-0.34	0.03	0.20	0.35	0.14	-0.11		
	θ_i^x	0.003	-0.08	1.58	0.05	1.89	-1.91	-1.15	-0.13		
	α_i^y	1.58	0.02	-0.02	0.23	0.06	-0.02				
	b_i^y	0.07	-0.37	0.10	0.24	-0.30	-0.64				
	θ_i^y	-0.004	-1.31	0.54	1.87	1.44	-1.08				
	α_i^z	0.04	-0.10	0.27	-0.08	-0.03	-0.01	0.02	-0.02	-0.05	
	b_i^z	-0.04	0.14	0.03	-0.28	-0.24	0.10	0.08	-0.04	0.15	
	θ_i^z	0.05	-0.20	-0.003	1.49	0.89	-1.48	-1.21	-0.38	1.86	

Table A1: The Gaussian parameters used for generating the artificial VCGs 1 through 5 are listed.

Record #	Index (i)	1	2	3	4	5	6	7	8	9	10	11
	α_i^x	1.11	-0.62	0.06	0.12	0.38	0.38	0.08	-0.05			
	b_i^x	0.08	-0.14	0.36	0.25	0.04	0.04	0.22	0.72			
	θ_i^x	-0.06	0.09	1.73	2.10	0.03	0.03	-1.14	-0.39			
	α_i^y	0.77	0.44	-0.04	0.02	0.09	0.10	-0.10				
patient155/s0301lre	b_i^y	0.06	0.06	0.91	0.21	0.24	0.22	0.20				
	θ_i^y	0.01	-0.11	-0.50	1.67	2.10	-1.28	-0.02				
	α_i^z	0.46	0.27	-0.07	-0.05	-0.08	0.04	0.53	0.07	0.18	-0.11	
	b_i^z	0.06	0.05	0.28	0.21	0.33	0.17	0.05	-0.89	0.10	0.06	
	θ_i^z	-0.09	0.12	0.60	1.72	1.22	-1.13	0.005	0.85	0.05	-0.31	
	α_i^x	0.03	0.08	-0.13	0.85	1.11	0.75	0.06	0.10	0.17	0.39	0.03
	b_i^x	0.09	0.11	0.05	0.04	0.03	0.03	0.04	0.60	0.30	0.18	0.50
	θ_i^x	-1.09	-0.83	-0.19	-0.07	0.00	0.06	0.22	1.20	1.42	1.68	2.90
	α_i^y	0.04	0.02	-0.02	0.32	0.51	-0.32	0.04	0.08	0.01		
patient165/s0323lre	b_i^y	0.07	0.07	0.04	0.06	0.04	0.06	0.45	0.30	0.50		
	θ_i^y	-1.10	-0.90	-0.76	-0.11	-0.01	0.07	0.80	1.58	2.90		
	α_i^z	-0.03	-0.14	-0.04	0.05	-0.40	0.46	-0.12	-0.20	-0.35	-0.04	
	b_i^z	0.03	0.12	0.04	0.40	0.05	0.05	0.80	0.40	0.20	0.40	
	θ_i^z	-1.10	-0.93	-0.70	-0.40	-0.15	0.10	1.05	1.25	1.55	2.80	
	α_i^x	0.03	-0.05	2.07	-0.87	0.38	0.14					
	b_i^x	0.13	0.48	0.08	0.12	0.23	0.38					
	θ_i^x	-1.30	-0.33	0.01	0.06	2.03	1.57					
	α_i^y	-0.10	1.95	-0.88	0.12	0.25	0.08	-0.04				
patient174/s0300lre	b_i^y	0.04	0.08	0.10	0.31	0.21	0.17	0.35				
	θ_i^y	-0.22	0.03	0.04	1.78	2.12	-1.44	-0.57				
	α_i^z	-0.21	0.46	0.23	-0.03	-0.07	-0.03	0.01				
	b_i^z	0.08	0.10	0.03	0.46	0.32	0.11	0.79				
	θ_i^z	-0.28	0.03	0.001	1.21	1.84	-1.72	-1.35				
	α_i^x	-0.04	1.97	-1.18	0.35	0.14	0.12					
	b_i^x	0.85	0.08	0.06	0.25	0.39	0.18					
	θ_i^x	-0.56	0.03	0.11	1.90	1.45	-1.14					
	α_i^y	-0.05	0.79	0.04	0.08	0.07	0.14	-0.06	0.33			
patient182/s0308lre	b_i^y	0.71	0.06	0.26	0.20	0.14	0.18	-0.03	0.04			
	θ_i^y	-0.89	0.01	1.50	1.87	2.12	-1.24	0.23	0.13			
	α_i^z	-0.45	0.38	0.04	-0.05	-0.14	0.02	-0.04				
	b_i^z	0.06	0.11	0.21	0.55	0.31	0.36	0.10				
	θ_i^z	-0.19	-0.03	2.12	1.06	1.73	-1.21	-1.45				
	α_i^x	0.53	1.20	-0.77	0.12	0.35	0.07	-0.03				
	b_i^x	0.03	0.07	0.10	0.39	0.23	0.14	-1.47				
	θ_i^x	0.08	0.01	0.11	1.49	1.93	-1.07	0.79				
	α_i^y	-0.04	0.78	-0.08	0.11	0.13	0.07					
patient185/s0336lre	b_i^y	0.61	0.05	0.07	0.24	0.18	0.12					
	θ_i^y	-0.35	-0.004	0.23	1.73	1.99	-1.15					
	α_i^z	-0.22	0.46	-0.01	0.09	-0.02	0.02	0.01				
	b_i^z	0.04	0.08	-0.59	0.02	0.09	0.14	0.08				
	θ_i^z	-0.21	0.03	-10.99	-0.02	-1.39	1.72	-1.10				

Table A2: The Gaussian parameters used for generating the artificial VCGs 6 through 10 are listed.

References

[1] N. Srinivasan and R. Schilling, "Sudden cardiac death and arrhythmias," *Arrhythmia and Electrophysiology Review*, vol. 7, pp. 111–117, Jul. 2018. DOI: 10.15420/aer.2018.15.2.

[2] C. Granger, R. Goldberg, and O. Dabbous, "Predictors of hospital mortality in the global registry of acute coronary events," *ACC Current Journal Review*, vol. 13, p. 13, Feb. 2004. DOI: 10.1016/j.accreview.2003.12.013.

[3] E. Antman, M. Cohen, P. Bernink, C. McCabe, T. Horacek, G. Papuchis, B. Mautner, R. Corbalan, D. Radley, and E. Braunwald, "The TIMI risk score for unstable angina/non-ST elevation MI: A method for prognostication and therapeutic decision making," *JAMA : The Journal of the American Medical Association*, vol. 284, pp. 835–42, Aug. 2000.

[4] Y. Liu, S. Zeeshan, B. Scirica, D. Morrow, J. Guttag, and C. Stultz, "ECG morphological variability in beat space for risk stratification after acute coronary syndrome," *Journal of the American Heart Association*, vol. 3, no. e000981, Apr. 2014. DOI: 10.1161/JAHA.114.000981.

[5] S. M. Narayan, "T-wave alternans and the susceptibility to ventricular arrhythmias," *Journal of the American College of Cardiology*, vol. 47, no. 2, pp. 269–281, 2006, ISSN: 0735-1097. DOI: https://doi.org/10.1016/j.jacc.2005.08.066.

[6] P. Brugada and J. Brugada, "Right bundle branch block, persistent ST segment elevation and sudden cardiac death: A distinct clinical and electrocardiographic syndrome," *Journal of the American College of Cardiology*, vol. 20, no. 6, pp. 1391–1396, 1992, ISSN: 0735-1097. DOI: http://dx.doi.org/10.1016/0735-1097(92)90253-J.

[7] B. D. Nearing and R. L. Verrier, "Modified moving average analysis of T-wave alternans to predict ventricular fibrillation with high accuracy," *Journal of Applied Physiology*, vol. 92, no. 2, pp. 541–549, 2002, PMID: 11796662. DOI: 10.1152/japplphysiol.00592.2001.

[8] J. Němec, "Nonalternans repolarization variability and arrhythmia - the calcium connection," *Journal of Electrocardiology*, vol. 49, pp. 877–882, Aug. 2016. DOI: 10.1016/j.jelectrocard.2016.08.003.

[9] J. Ramirez, M. Orini, D. Tucker, E. Pueyo, and P. Laguna, "Variability of ventricular repolarization dispersion quantified by time-warping the morphology of the T-waves," *IEEE Transactions on Biomedical Engineering*, vol. PP, no. 99, pp. 1619–1630, 2017, ISSN: 0018-9294. DOI: 10.1109/TBME.2016.2614899.

[10] M. S. Fuller, G. Sándor, B. Punske, B. Taccardi, R. S. MacLeod, P. R. Ershler, L. S. Green, and R. L. Lux, "Estimates of repolarization dispersion from electrocardiographic measurements," *Circulation*, vol. 102, no. 6, pp. 685–691, 2000, ISSN: 0009-7322. DOI: 10.1161/01.CIR.102.6.685.

[11] Z. Syed, B. Scirica, S. Mohanavelu, D. Morrow, C. Stutz, and J. Guttag, "Association of heart rate turbulence, deceleration capacity, and morphologic variability with sudden cardiac death following non-ST-elevation acute coronary syndrome: Results from the MERLIN-TIMI 36 trial," in *American Heart Association Annual Meeting*, 2010. DOI: 10.1161/circ.122.suppl_21.A15908.

[12] Z. Syed, B. Scirica, C. Stultz, and J. Guttag, "Electrocardiographic prediction of arrhythmias," in *2009 36th Annual Computers in Cardiology Conference (CinC)*, Published by Computers in Cardiology, 2009, pp. 741–744, ISBN: 9781424472819.

[13] B. E. Backus, A. J. Six, J. H. Kelder, W. B. Gibler, F. L. Moll, P. A. Doevendans, and M. E. H. Ong, "Risk scores for patients with chest pain: Evaluation in the emergency department," *Current Cardiology Reviews*, vol. 7, no. 1, pp. 2–8, Feb. 2011, ISSN: 1573403X. DOI: 10.2174/157340311795677662.

[14] P. Sung, Z. Syed, and J. Guttag, "Quantifying morphology changes in time series data with skew," in *2009 IEEE International Conference on Acoustics, Speech and Signal Processing*, IEEE, Apr. 2009, pp. 477–480, ISBN: 978-1-4244-2353-8. DOI: 10.1109/ICASSP.2009.4959624.

[15] H. Costin, C. Rotariu, and A. Pasarica, "Atrial fibrillation onset prediction using variability of ECG signals," *Proc. of the 8th Int. Symp. on Advanced Topics in Electrical Engineering (ATEE)*, May 2013. DOI: 10.1109/ATEE.2013.6563419.

[16] C.-C. Chia, M. Saeed, C. Stultz, J. Guttag, and Z. Syed, "Abstract 18756: Association of morphologic variability with 6-month mortality in a general cohort of intensive care unit patients: Results from the MIMICII database," *Circulation*, vol. 126, no. Suppl 21, A18756–A18756, 2016. DOI: 10.1161/circ.126.suppl_21.A18756.

[17] Z. Syed, B. M. Scirica, S. Mohanavelu, P. Sung, E. L. Michelson, C. P. Cannon, P. H. Stone, C. M. Stultz, and J. V. Guttag, "Relation of death within 90 days of non-ST-elevation acute coronary syndromes to variability in electrocardiographic morphology," *The American Journal of Cardiology*, vol. 103, no. 3, pp. 307–311, Feb. 2009, ISSN: 00029149. DOI: 10.1016/j.amjcard.2008.09.099.

[18] Z. Syed, B. M. Scirica, C. M. Stultz, and J. V. Guttag, "Risk-stratification following acute coronary syndromes using a novel electrocardiographic technique to measure variability in morphology," in *Computers in Cardiology*, vol. 35, IEEE, Sep. 2008, pp. 13–16, ISBN: 1424437067. DOI: 10.1109/CIC.2008.4748965.

[19] Z. Syed, C. M. Stultz, B. M. Scirica, C. P. Cannon, K. Attia, I. O. Stebletsova, S. Mohanavelu, P. H. Stone, and J. V. Guttag, "Abstract 2850: Morphological variability: A new electrocardiographic technique for risk stratification after NSTEACS," *Circulation*, vol. 116, no. Suppl 16, p. 634, 2015.

[20] M. Baumert, A. Porta, M. Vos, M. Malik, J.-P. Couderc, P. Laguna, G. Piccirillo, G. Smith, L. Tereshchenko, and P. Volders, "QT interval variability in body surface ECG: Measurement, physiological basis, and clinical value: Position statement and consensus guidance endorsed by the European Heart Rhythm Association jointly with the ESC working group on cardiac cellular electrophysiology," *EP Europace*, vol. 18, pp. 925–944, Jun. 2016. DOI: 10.1093/europace/euv405.

[21] A. Mincholé, E. Pueyo, J. F. Rodriguez, E. Zacur, M. Doblaré, and P. Laguna, "Quantification of restitution dispersion from the dynamic changes of the T-wave peak to end, measured at the surface ECG," *IEEE Transactions on Biomedical Engineering*, vol. 58, no. 5, pp. 1172–1182, May 2011, ISSN: 0018-9294. DOI: 10.1109/TBME.2010.2097597.

[22] S. Nemati, O. Abdala, V. Monasterio Bazán, S. Yim-Yeh, A. Malhotra, and G. D. Clifford, "A nonparametric surrogate-based test of significance for T-wave alternans detection," *IEEE Transactions on Biomedical Engineering*, vol. 58, pp. 1356–1364, Jun. 2011. DOI: 10.1109/TBME.2010.2047859.

[23] C. Lieber and V. Mohsenin, "Cheyne-Stokes respiration in congestive heart failure.," *The Yale Journal of Biology and Medicine*, vol. 65, no. 1, pp. 39–50, 1992.

[24] G. D. Clifford, "Advanced methods and tools for ECG data analysis," in. 685 Canton St. Norwood, MA 02062 United States: Artech House, 2006, ch. 3 "ECG Statistics, Noise, Artifacts, and Missing Data", pp. 55–99.

[25] R. Bailón, L. Sörnmo, and P. Laguna, "Advanced methods and tools for ECG data analysis," in. 685 Canton St. Norwood, MA 02062 United States: Artech House, 2006, ch. 8 "ECG-Derived Respiratory Frequency Estimation", pp. 215–244.

[26] S. Nemati, A. Malhotra, and G. D. Clifford, "T-wave alternans patterns during sleep in healthy, cardiac disease and sleep apnea patients," *Journal of Electrocardiology*, vol. 44, pp. 126–30, Dec. 2010. DOI: 10.1016/j.jelectrocard.2010.10.036.

[27] H. Sakoe and S. Chiba, "Dynamic programming algorithm optimization for spoken word recognition," *IEEE Transactions on Acoustics, Speech, and Signal Processing*, vol. 26, no. 1, pp. 43–49, 1978.

[28] M. J. Lisenby and P. C. Richardson, "The beatquency domain: An unusual application of the fast Fourier transform," *IEEE Transactions on Biomedical Engineering*, vol. BME-24, no. 4, pp. 405–408, Jul. 1977, ISSN: 1558-2531. DOI: 10.1109/TBME.1977.326155.

[29] G. D. Clifford, S. Nemati, and R. Sameni, "An artificial vector model for generating abnormal electrocardiographic rhythms," *Physiological Measurement*, vol. 31, pp. 595–609, Mar. 2010. DOI: 10.1088/0967-3334/31/5/001.

[30] L. Burattini, W. Zareba, J. P. Couderc, J. A. Konecki, and A. J. Moss, "Optimizing ECG signal sampling frequency for T-wave alternans detection," in *Computers in Cardiology 1998. Vol. 25 (Cat. No.98CH36292)*, Sep. 1998, pp. 721–724. DOI: 10.1109/CIC.1998.731975.

[31] J. Ben-Arie and K. R. Rao, "Nonorthogonal signal representation by Gaussians and Gabor functions," *IEEE Transactions on Circuits and Systems II: Analog and Digital Signal Processing*, vol. 42, no. 6, pp. 402–413, 1995.

[32] P. E. McSharry, G. D. Clifford, L. Tarassenko, and L. A. Smith, "A dynamical model for generating synthetic electrocardiogram signals," *IEEE Transactions on Biomedical Engineering*, vol. 50, no. 3, pp. 289–294, 2003.

[33] P. Davey, "A new physiological method for heart rate correction of the QT interval," *Heart*, vol. 82, no. 2, pp. 183–186, 1999, ISSN: 1355-6037. DOI: 10.1136/hrt.82.2.183.

[34] J. W. Mason, D. G. Strauss, M. Vaglio, and F. Badilini, "Correction of the QRS duration for heart rate," *Journal of Electrocardiology*, vol. 54, pp. 1–4, 2019, ISSN: 0022-0736. DOI: https://doi.org/10.1016/j.jelectrocard.2019.02.005.

[35] R. Sameni, G. D. Clifford, C. Jutten, and M. Shamsollahi, "Multichannel ECG and noise modeling: Application to maternal and fetal ECG signals," *EURASIP Journal on Advances in Signal Processing*, vol. 2007, no. 043407 (2007), Dec. 2007. DOI: 10.1155/2007/43407.

[36] A. Goldberger, L. Amaral, L. Glass, J. Hausdorff, P. Ivanov, R. Mark, J. Mietus, G. Moody, C.-K. Peng, and H. Stanley, "Physiobank, Physiotoolkit, and Physionet : Components of a new research resource for complex physiologic signals," *Circulation*, vol. 101, E215–20, Jul. 2000. DOI: 10.1161/01.CIR.101.23.e215.

[37] *Normal Sinus Rhythm database*, 1999 (accessed September 3, 2019). DOI: https://doi.org/10.13026/C2NK5R. [Online]. Available: https://www.physionet.org/content/nsrdb/1.0.0/.

[38] R. Costin, C. Rotariu, and A. Pasarica, "Mental stress detection using heart rate variability and morphologic variability of ECG signals," in *2012 International Conference and Exposition on Electrical and Power Engineering*, 2012, pp. 591–596. DOI: 10.1109/ICEPE.2012.6463870.

[39] R. Lampert, "ECG signatures of psychological stress," *Journal of Electrocardiology*, vol. 48, pp. 1000–1005, Sep. 2015. DOI: 10.1016/j.jelectrocard.2015.08.005.

[40] P. Chazal, M. O'Dwyer, and R. Reilly, "Automatic classification of heartbeats using ECG morphology and heartbeat interval features," *IEEE Transactions on Biomedical Engineering*, vol. 51, pp. 1196–206, Aug. 2004. DOI: 10.1109/TBME.2004.827359.

[41] J. P. Martinez, R. Almeida, S. Olmos, A. P. Rocha, and P. Laguna, "A wavelet-based ECG delineator: Evaluation on standard databases," *IEEE Transactions on Biomedical Engineering*, vol. 51, no. 4, pp. 570–581, Apr. 2004, ISSN: 0018-9294. DOI: 10.1109/TBME.2003.821031.

[42] Q. Li, C. Rajagopalan, and G. D. Clifford, "A machine learning approach to multi-level ECG signal quality classification," *Computer Methods and Programs in Biomedicine*, vol. 117, pp. 435–447, Sep. 2014. DOI: 10.1016/j.cmpb.2014.09.002.

[43] R. L. Verrier, K. Kumar, and B. D. Nearing, "Basis for sudden cardiac death prediction by T-wave alternans from an integrative physiology perspective," *Heart Rhythm : the official Journal of the Heart Rhythm Society*, vol. 6, pp. 416–22, Apr. 2009. DOI: 10.1016/j.hrthm.2008.11.019.

[44] P. Charlton, T. Bonnici, L. Tarassenko, D. Clifton, R. Beale, and P. Watkinson, "An assessment of algorithms to estimate respiratory rate from the electrocardiogram and photoplethysmogram," *Physiological Measurement*, vol. 37, pp. 610–626, Mar. 2016. DOI: 10.1088/0967-3334/37/4/610.

[45] A. Schäfer and K. Kratky, "Estimation of breathing rate from respiratory sinus arrhythmia: Comparison of various methods," *Annals of Biomedical Engineering*, vol. 36, pp. 476–85, Apr. 2008. DOI: 10.1007/s10439-007-9428-1.

[46] W. Karlen, S. Raman, J. M. Ansermino, and G. A. Dumont, "Multiparameter respiratory rate estimation from the photoplethysmogram," *IEEE Transactions on Biomedical Engineering*, vol. 60, no. 7, pp. 1946–1953, 2013.

[47] R. Verrier, T. Klingenheben, M. Malik, N. El-Sherif, D. V Exner, S. H Hohnloser, T. Ikeda, J. P. Martínez, S. M Narayan, T. Nieminen, and D. S Rosenbaum, "Microvolt T-wave alternans physiological basis, methods of measurement, and clinical utility-consensus guideline by international society for Holter and noninvasive electrocardiology," *Journal of the American College of Cardiology*, vol. 58, pp. 1309–24, Sep. 2011. DOI: 10.1016/j.jacc.2011.06.029.

[48] S. Nemati, A. Malhotra, and G. D. Clifford, "Data fusion for improved respiration rate estimation," *EURASIP J. Adv. Signal Process*, vol. 2010, no. 926305 (2010), Feb. 2010, ISSN: 1110-8657. DOI: 10.1155/2010/926305. [Online]. Available: https://doi.org/10.1155/2010/926305.

[49] A. N. Vest, G. D. Poian, Q. Li, C. Liu, S. Nemati, A. J. Shah, and G. D. Clifford, "An open source benchmarked toolbox for cardiovascular waveform and interval analysis," *Physiological Measurement*, vol. 39, no. 10, p. 105 004, Oct. 2018a. DOI: 10.1088/1361-6579/aae021.

[50] ——, *Physionet Cardiovascular Signal Toolbox*, 2018b. DOI: 10.5281/zenodo.1243111.

[51] G. B. Moody, R. G. Mark, A. Zoccola, and S. Mantero, "Derivation of respiratory signals from multilead ECGs," *Computers in Cardiology*, vol. 12, pp. 113–116, 1985.

[52] J. Leino, M. Minkkinen, T. Nieminen, T. Lehtimäki, J. Viik, R. Lehtinen, K. Nikus, T. Kööbi, V. Turjanmaa, R. Verrier, and M. Kähönen, "Combined assessment of heart rate recovery and T-wave alternans during routine exercise testing improves prediction of total and cardiovascular mortality: The Finnish Cardiovascular Study," *Heart Rhythm : the official Journal of the Heart Rhythm Society*, vol. 6, pp. 1765–71, Dec. 2009. DOI: 10.1016/j.hrthm.2009.08.015.

[53] W. Einthoven, G. Fahr, and A. de Waart, "On the direction and manifest size of the variations of potential in the human heart and on the influence of the position of the heart on the form of the electrocardiogram," *American Heart Journal*, vol. 40, no. 2, pp. 163–211, 1950, ISSN: 0002-8703. DOI: https://doi.org/10.1016/0002-8703(50)90165-7.

[54] C. Funck-Brentano and P. Jaillon, "Rate-corrected QT interval: Techniques and limitations," *The American Journal of Cardiology*, vol. 72, 17B–22B, Sep. 1993. DOI: 10.1016/0002-9149(93)90035-B.

[55] R. Bailón, L. Sörnmo, and P. Laguna, "A robust method for ECG-based estimation of the respiratory frequency during stress testing," *IEEE Transactions on Biomedical Engineering*, vol. 53, pp. 1273–85, Aug. 2006. DOI: 10.1109/TBME.2006.871888.

[56] G. B. Moody, W. E. Muldrow, and R. G. Mark, "A noise stress test for arrhythmia detectors," *Computers in Cardiology*, vol. 11, pp. 381–384, 1984. DOI: https://doi.org/10.13026/C2HS3T.

[57] R. Bousseljot, D. Kreiseler, and A. Schnabel, "Nutzung der EKG-Signaldatenbank CARDIODAT der PTB über das Internet," *Biomedizinische Technik - BIOMED TECH*, vol. 40, pp. 317–318, Jan. 1995. DOI: https://doi.org/10.13026/C28C71.

[58] R. Sameni, *The open-source electrophysiological toolbox (OSET), version 2.1*, 2010 (accessed July 15, 2017). [Online]. Available: https://gitlab.com/rsameni/OSET.git.